INVESTIGATION OF HUMAN CORTICAL ACTIVITY WITH MICROELECTRODE ARRAYS DURING ANESTHESIA AND MOVEMENT

by

Sara Hanrahan

A dissertation submitted to the faculty of
The University of Utah
in partial fulfillment of the requirements for the degree of

Doctor of Philosophy

Department of Bioengineering

The University of Utah

December 2014

The University of Utah Graduate School

STATEMENT OF DISSERTATION APPROVAL

The dissertation of **Sara Hanrahan**

has been approved by the following supervisory committee members:

Bradley Greger	, Chair	**04/02/2014** Date Approved
Paul House	, Member	**07/07/2014** Date Approved
Richard Normann	, Member	**07/10/2014** Date Approved
Alan Dale Dorval II	, Member	**07/09/2014** Date Approved
Florian Solzbacher	, Member	**07/16/2014** Date Approved

and by **Patrick Tresco** , Chair/Dean of

the Department/College/School of **Bioengineering**

and by David B. Kieda, Dean of The Graduate School.

ABSTRACT

Recording the neural activity of human subjects is indispensable for fundamental neuroscience research and clinical applications. Human studies range from examining the neural activity of large regions of the cortex using electroencephalography (EEG) or electrocorticography (ECoG) to single neurons or small populations of neurons using microelectrode arrays. In this dissertation, microscale recordings in the human cortex were analyzed during administration of propofol anesthesia and articulate movements such as speech, finger flexion, and arm reach. Recordings were performed on epilepsy patients who required long-term electrocorticographic monitoring and were implanted with penetrating or surface microelectrode arrays.

We used penetrating microelectrode arrays to investigate the effects of propofol anesthesia on action potentials (APs) and local field potentials (LFPs). Increased propofol concentration correlated with decreased high-frequency power in LFP spectra and decreased AP firing rates, as well as the generation of large amplitude spike-like LFP activity; however, the temporal relationship between APs and LFPs remained relatively consistent at all levels of propofol anesthesia. The propofol-induced suppression of neocortical network activity allowed LFPs to be dominated by low-frequency spike-like activity, and correlated with sedation and unconsciousness. As the low-frequency spike-like activity increased, and the AP-LFP relationship became more predictable, firing rate

encoding capacity was impaired. This suggests a mechanism for decreased information processing in the neocortex that accounts for propofol-induced unconsciousness.

We also demonstrated that speech, finger, and arm movements can be decoded from LFPs recorded with dense grids of microelectrodes placed on the surface of human cerebral cortex for brain computer interface (BCI) applications using LFPs recorded over face-motor area, vocalized articulations of ten different words and silence were classified on a trial-by-trial basis with 82.4% accuracy. Using LFPs recorded over the hand area of motor cortex, three individual finger movements and rest were classified on a trial-by-trial basis with 62% accuracy. LFPs recorded over the arm area of motor cortex were used to continuously decode the arm trajectory with a maximum correlation coefficient of 0.82 in the x-direction and 0.76 in the y-direction. These findings demonstrate that LFPs recorded by micro-ECoG grids from the surface of the cerebral cortex contain sufficient information to provide rapid and intuitive control a BCI communication or motor prosthesis.

TABLE OF CONTENTS

LIST OF FIGURES

LIST OF TABLES

CHAPTER 1

INTRODUCTION

Recording the neural activity of human subjects is indispensable for fundamental neuroscience research and clinical applications. Human neural recordings allow us to extend established neuroscience studies in animals and to address the mechanisms of higher cognitive functions not found in animals. Human studies range from examining the neural activity of large regions of the brain using grids of electrodes such as electroencephalography (EEG) or electrocorticography (ECoG) to assessing the neural activity of single neurons or small populations of neurons using microelectrode arrays. In this dissertation, microscale recordings in the human cortex are examined during propofol anesthesia and articulate movements such as speech, finger flexion, and arm reach.

1.1 Background

1.1.1 Electroencephalography

Researchers have a variety of tools to choose from when studying brain function. Assessing cortical electrical activity originated with the development of EEG by Hans Berger (Berger 1929). EEG grids are electrodes placed on the scalp surface to record cortical activity noninvasively. EEG continues to be used by many researchers to

examine neural activity during different cognitive states or behavioral tasks. EEG can provide a global assessment of cortical activity, but has prohibitively low temporal and spatial resolution.

Specifically, EEG has been used globally to assess neural activity during the administration of propofol anesthesia and motor control. With increased propofol administration in human subjects, EEG investigations demonstrate that cortical activity shifts from a high-frequency, low-amplitude signal to a low-frequency, high-amplitude signal (Feshchenko et al. 2004). As propofol concentration is further increased, the EEG signal develops a burst suppression pattern with flat low-amplitude periods interspaced between high alpha and beta activity (Clark and Rosner 1973) and at the highest levels of propofol sedation, the EEG signal becomes isoelectric (Claassen et al. 2002). Alternatively, brain computer interface (BCI) studies have shown that human subjects can use signals recorded with EEG to indirectly communicate by spelling words (Birbaumer et al. 1999; Schalk et al. 2004), to move a computer cursor (Felton et al. 2009; Huang et al. 2009; Wolpaw and McFarland 2004), and to provide 1-Dimensional control of a prosthetic arm (Hazrati and Erfanian 2010; Lauer et al. 1999; Pfurtscheller et al. 2000). Although EEG signals can provide information on the effects of propofol on a global scale, EEG signals cannot provide the fine-scale resolution necessary for intuitive control of a prosthetic device.

1.1.2 Electrocorticography

ECoG has become common for recording neural activity in human subjects because of its clinical ubiquity in preparing patients for the surgical treatment of epilepsy (Feindel

et al. 1952). For patients who have medically refractory epilepsy, ECoG grids are placed on the surface of the cortex for a one- to two-week period to localize the epileptogenic zone and eloquent cortex (Figure 1.1A). Patients volunteer for neurophysiological research studies and their neural activity is recorded during their hospital stay while they are in different cognitive states or perform behavioral tasks. Because ECoG electrodes are closer to the desired signals, they can record neural signals with a higher signal-to-noise ratio and higher spatial resolution than EEG (Buzsaki et al. 2012; Cooper 1965).

Specifically, ECoG has been used to assess neural activity during propofol anesthesia and motor control. With the induction of anesthesia, the neural activity recorded with ECoG electrodes increased in delta band (1–2 Hz) power and decreased in gamma band (37–205 Hz) power. In addition, the correlation between the phase of the delta band (1–4 Hz) and the power of the gamma band (23–165 Hz) strengthened with propofol anesthesia (Breshears et al. 2010). For BCI studies, neural activity recorded from ECoG electrodes has been used in the classification of spoken words or phonemes (Blakely et al. 2008; Chang et al. 2010; Leuthardt et al. 2004), classification of finger movements (Chestek et al. 2013; Kubanek et al. 2009; Miller et al. 2012; Miller et al. 2009; Pistohl et al. 2012) and continuous decoding of arm movement (Chao et al. 2010; Ganguly et al. 2009; Pistohl et al. 2008; Pistohl et al. 2013; Sanchez et al. 2008; Schalk et al. 2008). With training periods of many days, cortical signals recorded with ECoG over sensorimotor cortex were able to provide a patient with tetraplegia limited control of a prosthetic arm (Wang et al. 2013). ECoG recordings in human cortex are limited to one or two electrodes modulating with a specific movement (Leuthardt et al. 2004; Menon et al. 1996; Milekovic et al. 2012). Because of this, some ECoG studies use indirect,

nonintuitive signals such as the movement of the tongue to control a computer cursor (Leuthardt et al. 2004; Schalk et al. 2008). ECoG electrodes are typically millimeters in diameter with interelectrode spacing on the centimeter-scale. ECoG grids likely spatially integrate and under-samples the information represented in the cerebral cortex at the scale of cortical columns. To examine the effects of propofol anesthesia on single neurons and small populations of neurons as well as decode neural activity during articulate movements, higher spatial resolution recording technology is necessary.

1.1.3 Microelectrodes

Microelectrode arrays have the ability to record highly localized neural activity. Both surface and penetrating microelectrode arrays are able to record microscale LFPs from a small population of neurons. LFPs recorded with high-impedance microelectrodes are thought to be generated by synaptic potentials (Katzner et al. 2009; Khawaja et al. 2009; Mitzdorf 1985; Nunez and Srinivasan 2006). While the spatial extent of LFPs are debated, they likely represent coordinated neural activity of cortical microcircuits, e.g., cortical columns (Mountcastle 1978). High-impedance electrodes have a limited recording radius and record neural signals with minimal spatial integration (Tsanov et al. 2011). Therefore, microelectrode arrays can have smaller interelectrode spacing and prevent the issue of under-sampling cortical activity.

Penetrating microelectrode arrays, unlike EEG and ECoG, are able to record APs from individual neurons and microscale LFPs (Figure 1.1B) (Buzsaki et al. 2012). The first report of successful single-unit recording in the human neocortex was in 1955 (Ward and Thomas 1955). Penetrating microelectrode arrays have been successfully implanted

and used for research applications in the motor cortex (Bansal et al. 2012; Egan et al. 2012; Gilja et al. 2012; Reimer and Hatsopoulos 2010; Velliste et al. 2008), auditory cortex (Rousche and Normann 1998; Smith et al. 2013), auditory nerve (Hillman et al. 2003; Middlebrooks and Snyder 2008), sciatic nerve (McDonnall et al. 2004), and visual cortex (Davis et al. 2012; Shushruth et al. 2011; Warren et al. 2001) of various animal models. Moreover, they have been acutely implanted in the middle temporal gyrus of epilepsy patients undergoing temporal lobectomy surgery (House et al. 2006; Keller et al. 2010; Schevon et al. 2010; Waziri et al. 2009). While many studies have demonstrated the utility of penetrating microelectrode arrays in many applications, the following research is one of two studies to show the effects of propofol anesthesia in humans. Penetrating microelectrode arrays were specifically used to examine AP-LFP relationships in human cortex.

Patients with tetraplegia have participated in BCI clinical trials with implanted penetrating microelectrode arrays. These arrays record APs from individual neurons in motor cortex for volitional control of a prosthetic arm (Collinger et al. 2013; Hochberg et al. 2012). Similar patients have used neural signals from penetrating microelectrode arrays to control a computer cursor to type and indirectly communicate (Kim et al. 2011). Due to an increased risk, few penetrating electrodes have been placed in the language areas of patients. One such study used a glass electrode filled with neurotrophic growth factor to encourage axonal growth into the electrode. The glass electrode was placed over the speech motor cortex to decode phonemes in real time (Guenther et al. 2009). Penetrating arrays are more invasive and AP recordings degrade over time (Polikov et al. 2005; Turner et al. 1999). This signal degradation may limit the lifetime of these BCI

systems. For BCI studies in which the penetrating microelectrode arrays were implanted for more than a year, AP sorting was hindered due to decreased AP amplitudes and threshold-crossing events were applied to the 2-Dimensional decodes instead (Chestek et al. 2011; Fraser et al. 2009).

The micro-ECoG grid was designed to record microscale LFPs at a high spatiotemporal resolution with invasiveness equivalent to an ECoG grid (Figure 1.1C). Micro-ECoG electrodes have a small surface area and high impedance, and therefore can record neural signals from a small volume of neural tissue. To avoid signal distortion, LFPs from micro-ECoG grids must be recorded by a high impedance amplifier, not a clinical ECoG recording system (Stacey et al. 2012). Unlike signals recorded from penetrating microelectrode arrays, LFPs recorded from the surface of the cortex may be less prone to signal degradation over time (Schendel et al. 2013). The tighter interelectrode spacing of micro-ECoG grids provides the ability to sample the closely spaced areas of motor cortex that control specific movements (Chestek et al. 2013; Crone 2006; Kim et al. 2007; Leuthardt et al. 2009; Menon et al. 1996; Miller et al. 2007; Slutzky et al. 2010; Van Gompel et al. 2008; Worrell et al. 2008). In previous studies, micro-ECoG grids have shown promise for decoding speech (Kellis et al. 2010; Leuthardt et al. 2011), arm movement (Kellis et al. 2009) and primary hand movements (Leuthardt et al. 2009).

1.2 Overview

In Chapter 2, we examined the electrophysiological response to propofol anesthesia, the most widely used intravenous general anesthetic for induction and maintenance of

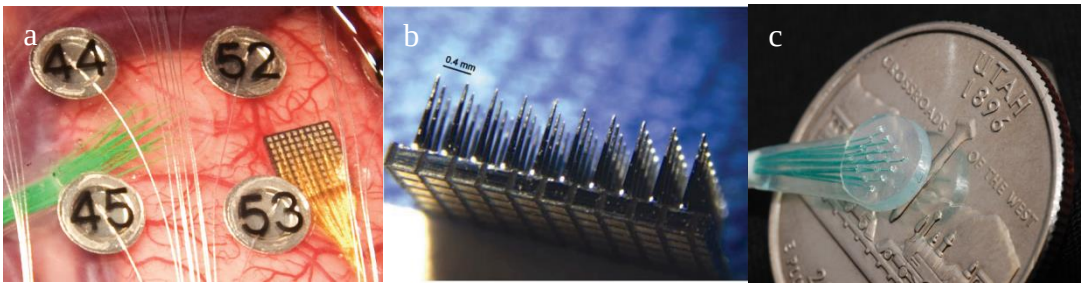

Figure 1.1. Electrode types used to record neocortical activity in human subjects. (a) Photograph of ECoG electrodes (silver disks with numbers), micro-ECoG electrodes (green wires) and penetrating microelectrode array (gold and brown square) implanted in human cortex. (b) Photograph of penetrating microelectrode array (Blackrock Microsystems), which was used to record neural data in Chapter 2. (c) Photograph of micro-ECoG grid (PMT Corporation), which was used to record neural data in Chapter 3.

anesthesia (Kotani et al. 2008). This study has important implications for the processing of information in the neocortex, and therefore on the interpretation of experimental results in anesthetized preparations and clinical results in intraoperative cortical mapping. While the pharmacology and EEG effects of propofol have been extensively studied, its effects on APs and LFPs are not well understood.

Propofol is an intravenous sedative hypnotic and is an allosteric modulator of $GABA_A$ chloride channels, which are more densely located in the neocortex than in subcortical structures. Therefore, propofol inhibits neural activity preferentially in the neocortex (Bai et al. 1999; Hentschke et al. 2005; Kaisti et al. 2002; Solt and Forman 2007). EEG and ECoG investigations have demonstrated that increasing propofol concentration in human subjects shifts cortical activity from a high-frequency, low-amplitude signal to a low-frequency, high-amplitude signal (Breshears et al. 2010; Feshchenko et al. 2004). Other studies have demonstrated that power in the high-frequency component of EEG signals corresponds to corticocortical activity (Gray and McCormick 1996), while power in the low-frequency component of EEG signals primarily arises from subcortical interactions (McCormick and Bal 1997). The decrease

in high-frequency power with the administration of propofol may be due to a decrease in intracortical and corticocortical activity. Alternatively, the increase in low-frequency power may arise from interactions with subcortical structures such as the thalamus (Ching et al. 2010; Velly et al. 2007). The use of microelectrode arrays allowed us to determine if this pattern was consistent at the level of individual neurons and small populations of neurons. We examined the effects of propofol anesthesia on APs, LFPs, and the temporal relationship between the two neural signals.

In Chapter 3, we used micro-ECoG grids to microscale LFPs for BCI applications. BCIs have the potential to help restore communication and motor function to patients suffering from neurological disorders. Amyotrophic lateral sclerosis (ALS) or spinal cord injury may leave patients severely paralyzed and unable to speak or interact with their environment in a condition known as locked-in syndrome (Smith and Delargy 2005). Some patients with locked-in syndrome depend on small residual movements for slow, basic communication and caregivers for physical interaction with their environment. By directly interfacing with the motor areas of the cortex, it may be possible to provide intuitive communication and environmental control (Birbaumer 2006). The field of BCIs relies on prior basic neuroscience literature that has characterized neural activity with force, position, and velocity during movement in monkeys (Evarts 1968; Georgopoulos et al. 1982). BCI systems transform neural activity related to intended movements into control signals for communication systems or assistive devices such as prosthetic arms. Ideally, the neural activity will be acquired with the highest spatial and temporal resolution possible, while using the most minimally invasive electrodes, in order to provide intuitive and reliable control.

This work extends previous studies in which similar micro-ECoG grids have been shown to support high temporal- and spatial-resolution recordings for BCI-like applications (Kellis et al. 2012; Kellis et al. 2010; Kellis et al. 2009). We used LFPs recorded on micro-ECoG grids placed over primary motor cortex to classify spoken word and individual finger movements, and to continuously decode the position of the hand during reaching.

1.3 References

Bai D, Pennefather PS, MacDonald JF, and Orser BA. The General Anesthetic Propofol Slows Deactivation and Desensitization of Gaba(a) Receptors. *J Neurosci* 19: 10635-10646, 1999.

Bansal AK, Truccolo W, Vargas-Irwin CE, and Donoghue JP. Decoding 3d Reach and Grasp from Hybrid Signals in Motor and Premotor Cortices: Spikes, Multiunit Activity, and Local Field Potentials. *J Neurophysiol* 107: 1337-1355, 2012.

Berger H. Über Das Elektrenkephalogramm Des Menschen. *Arch Psychiatr Nervenkr* 87: 527–570 1929.

Birbaumer N. Breaking the Silence: Brain-Computer Interfaces (Bci) for Communication and Motor Control. *Psychophysiology* 43: 517-532, 2006.

Birbaumer N, Ghanayim N, Hinterberger T, Iversen I, Kotchoubey B, Kubler A, Perelmouter J, Taub E, and Flor H. A Spelling Device for the Paralysed. *Nature* 398: 297-298, 1999.

Blakely T, Miller KJ, Rao RP, Holmes MD, and Ojemann JG. Localization and Classification of Phonemes Using High Spatial Resolution Electrocorticography (Ecog) Grids. *Conf Proc IEEE Eng Med Biol Soc* 2008: 4964-4967, 2008.

Breshears JD, Roland JL, Sharma M, Gaona CM, Freudenburg ZV, Tempelhoff R, Avidan MS, and Leuthardt EC. Stable and Dynamic Cortical Electrophysiology of Induction and Emergence with Propofol Anesthesia. *Proc Natl Acad Sci U S A* 107: 21170-21175, 2010.

Buzsaki G, Anastassiou CA, and Koch C. The Origin of Extracellular Fields and Currents--Eeg, Ecog, Lfp and Spikes. *Nat Rev Neurosci* 13: 407-420, 2012.

Chang EF, Rieger JW, Johnson K, Berger MS, Barbaro NM, and Knight RT. Categorical Speech Representation in Human Superior Temporal Gyrus. *Nat Neurosci* 13: 1428-1432, 2010.

Chao ZC, Nagasaka Y, and Fujii N. Long-Term Asynchronous Decoding of Arm Motion Using Electrocorticographic Signals in Monkeys. *Front Neuroeng* 3: 3, 2010.

Chestek CA, Gilja V, Blabe CH, Foster BL, Shenoy KV, Parvizi J, and Henderson JM. Hand Posture Classification Using Electrocorticography Signals in the Gamma Band over Human Sensorimotor Brain Areas. *J Neural Eng* 10: 026002, 2013.

Chestek CA, Gilja V, Nuyujukian P, Foster JD, Fan JM, Kaufman MT, Churchland MM, Rivera-Alvidrez Z, Cunningham JP, Ryu SI, and Shenoy KV. Long-Term Stability of Neural Prosthetic Control Signals from Silicon Cortical Arrays in Rhesus Macaque Motor Cortex. *J Neural Eng* 8: 045005, 2011.

Ching S, Cimenser A, Purdon PL, Brown EN, and Kopell NJ. Thalamocortical Model for a Propofol-Induced Alpha-Rhythm Associated with Loss of Consciousness. *Proc Natl Acad Sci U S A* 107: 22665-22670, 2010.

Claassen J, Hirsch LJ, Emerson RG, and Mayer SA. Treatment of Refractory Status Epilepticus with Pentobarbital, Propofol, or Midazolam: A Systematic Review. *Epilepsia* 43: 146-153, 2002.

Clark DL, and Rosner BS. Neurophysiologic Effects of General Anesthetics. I. The Electroencephalogram and Sensory Evoked Responses in Man. *Anesthesiology* 38: 564-582, 1973.

Collinger JL, Wodlinger B, Downey JE, Wang W, Tyler-Kabara EC, Weber DJ, McMorland AJ, Velliste M, Boninger ML, and Schwartz AB. High-Performance Neuroprosthetic Control by an Individual with Tetraplegia. *Lancet* 381: 557-564, 2013.

Cooper R, et al. Comparison of Subcortical, Cortical and Scalp Activity Using Chronically Indwelling Electrodes in Man. *Electroencephalogr Clin Neurophysiol* 18: 217-228, 1965.

Crone N, Sinai, A., Korzeniewska, A. *Event-Related Dynamics of Brain Oscillations*. Elsevier, 2006.

Davis TS, Parker RA, House PA, Bagley E, Wendelken S, Normann RA, and Greger B. Spatial and Temporal Characteristics of V1 Microstimulation During Chronic Implantation of a Microelectrode Array in a Behaving Macaque. *J Neural Eng* 9: 065003, 2012.

Egan J, Baker J, House PA, and Greger B. Decoding Dexterous Finger Movements in a Neural Prosthesis Model Approaching Real-World Conditions. *IEEE Trans Neural Syst Rehabil Eng* 20: 836-844, 2012.

Evarts EV. Relation of Pyramidal Tract Activity to Force Exerted During Voluntary Movement. *J Neurophysiol* 31: 14-27, 1968.

Feindel W, Penfield W, and Jasper H. Localization of Epileptic Discharge in Temporal Lobe Automatism. *Trans Am Neurol Assoc* 56: 14-17, 1952.

Felton EA, Radwin RG, Wilson JA, and Williams JC. Evaluation of a Modified Fitts Law Brain-Computer Interface Target Acquisition Task in Able and Motor Disabled Individuals. *J Neural Eng* 6: 056002, 2009.

Feshchenko VA, Veselis RA, and Reinsel RA. Propofol-Induced Alpha Rhythm. *Neuropsychobiology* 50: 257-266, 2004.

Fraser GW, Chase SM, Whitford A, and Schwartz AB. Control of a Brain-Computer Interface without Spike Sorting. *J Neural Eng* 6: 055004, 2009.

Ganguly K, Secundo L, Ranade G, Orsborn A, Chang EF, Dimitrov DF, Wallis JD, Barbaro NM, Knight RT, and Carmena JM. Cortical Representation of Ipsilateral Arm Movements in Monkey and Man. *J Neurosci* 29: 12948-12956, 2009.

Georgopoulos AP, Kalaska JF, Caminiti R, and Massey JT. On the Relations between the Direction of Two-Dimensional Arm Movements and Cell Discharge in Primate Motor Cortex. *J Neurosci* 2: 1527-1537, 1982.

Gilja V, Nuyujukian P, Chestek CA, Cunningham JP, Yu BM, Fan JM, Churchland MM, Kaufman MT, Kao JC, Ryu SI, and Shenoy KV. A High-Performance Neural Prosthesis Enabled by Control Algorithm Design. *Nat Neurosci* 15: 1752-1757, 2012.

Gray CM, and McCormick DA. Chattering Cells: Superficial Pyramidal Neurons Contributing to the Generation of Synchronous Oscillations in the Visual Cortex. *Science* 274: 109-113, 1996.

Guenther FH, Brumberg JS, Wright EJ, Nieto-Castanon A, Tourville JA, Panko M, Law R, Siebert SA, Bartels JL, Andreasen DS, Ehirim P, Mao H, and Kennedy PR. A Wireless Brain-Machine Interface for Real-Time Speech Synthesis. *PLoS One* 4: e8218, 2009.

Hazrati M, and Erfanian A. An Online Eeg-Based Brain-Computer Interface for Controlling Hand Grasp Using an Adaptive Probabilistic Neural Network. *Med Eng Phys* 32: 730-739, 2010.

Hentschke H, Schwarz C, and Antkowiak B. Neocortex Is the Major Target of Sedative Concentrations of Volatile Anaesthetics: Strong Depression of Firing Rates and Increase of Gabaa Receptor-Mediated Inhibition. *Eur J Neurosci* 21: 93-102, 2005.

Hillman T, Badi AN, Normann RA, Kertesz T, and Shelton C. Cochlear Nerve Stimulation with a 3-Dimensional Penetrating Electrode Array. *Otol Neurotol* 24: 764-768, 2003.

Hochberg LR, Bacher D, Jarosiewicz B, Masse NY, Simeral JD, Vogel J, Haddadin S, Liu J, Cash SS, van der Smagt P, and Donoghue JP. Reach and Grasp by People with Tetraplegia Using a Neurally Controlled Robotic Arm. *Nature* 485: 372-375, 2012.

House PA, MacDonald JD, Tresco PA, and Normann RA. Acute Microelectrode Array Implantation into Human Neocortex: Preliminary Technique and Histological Considerations. *Neurosurg Focus* 20: E4, 2006.

Huang D, Lin P, Fei DY, Chen X, and Bai O. Decoding Human Motor Activity from Eeg Single Trials for a Discrete Two-Dimensional Cursor Control. *J Neural Eng* 6: 046005, 2009.

Kaisti KK, Metsahonkala L, Teras M, Oikonen V, Aalto S, Jaaskelainen S, Hinkka S, and Scheinin H. Effects of Surgical Levels of Propofol and Sevoflurane Anesthesia on Cerebral Blood Flow in Healthy Subjects Studied with Positron Emission Tomography. *Anesthesiology* 96: 1358-1370, 2002.

Katzner S, Nauhaus I, Benucci A, Bonin V, Ringach DL, and Carandini M. Local Origin of Field Potentials in Visual Cortex. *Neuron* 61: 35-41, 2009.

Keller CJ, Truccolo W, Gale JT, Eskandar E, Thesen T, Carlson C, Devinsky O, Kuzniecky R, Doyle WK, Madsen JR, Schomer DL, Mehta AD, Brown EN, Hochberg LR, Ulbert I, Halgren E, and Cash SS. Heterogeneous Neuronal Firing Patterns During Interictal Epileptiform Discharges in the Human Cortex. *Brain* 133: 1668-1681, 2010.

Kellis S, Hanrahan S, Davis T, House PA, Brown R, and Greger B. Decoding Hand Trajectories from Micro-Electrocorticography in Human Patients. *Conf Proc IEEE Eng Med Biol Soc* 2012: 4091-4094, 2012.

Kellis S, Miller K, Thomson K, Brown R, House P, and Greger B. Decoding Spoken Words Using Local Field Potentials Recorded from the Cortical Surface. *J Neural Eng* 7: 056007, 2010.

Kellis SS, House PA, Thomson KE, Brown R, and Greger B. Human Neocortical Electrical Activity Recorded on Nonpenetrating Microwire Arrays: Applicability for Neuroprostheses. *Neurosurg Focus* 27: E9, 2009.

Khawaja FA, Tsui JM, and Pack CC. Pattern Motion Selectivity of Spiking Outputs and Local Field Potentials in Macaque Visual Cortex. *J Neurosci* 29: 13702-13709, 2009.

Kim J, Wilson JA, and Williams JC. A Cortical Recording Platform Utilizing Microecog Electrode Arrays. *Conf Proc IEEE Eng Med Biol Soc* 2007: 5353-5357, 2007.

Kim SP, Simeral JD, Hochberg LR, Donoghue JP, Friehs GM, and Black MJ. Point-and-Click Cursor Control with an Intracortical Neural Interface System by Humans with Tetraplegia. *IEEE Trans Neural Syst Rehabil Eng* 19: 193-203, 2011.

Kotani Y, Shimazawa M, Yoshimura S, Iwama T, and Hara H. The Experimental and Clinical Pharmacology of Propofol, an Anesthetic Agent with Neuroprotective Properties. *CNS Neurosci Ther* 14: 95-106, 2008.

Kubanek J, Miller KJ, Ojemann JG, Wolpaw JR, and Schalk G. Decoding Flexion of Individual Fingers Using Electrocorticographic Signals in Humans. *J Neural Eng* 6: 066001, 2009.

Lauer RT, Peckham PH, and Kilgore KL. Eeg-Based Control of a Hand Grasp Neuroprosthesis. *Neuroreport* 10: 1767-1771, 1999.

Leuthardt EC, Freudenberg Z, Bundy D, and Roland J. Microscale Recording from Human Motor Cortex: Implications for Minimally Invasive Electrocorticographic Brain-Computer Interfaces. *Neurosurg Focus* 27: E10, 2009.

Leuthardt EC, Gaona C, Sharma M, Szrama N, Roland J, Freudenberg Z, Solis J, Breshears J, and Schalk G. Using the Electrocorticographic Speech Network to Control a Brain-Computer Interface in Humans. *J Neural Eng* 8: 036004, 2011.

Leuthardt EC, Schalk G, Wolpaw JR, Ojemann JG, and Moran DW. A Brain-Computer Interface Using Electrocorticographic Signals in Humans. *J Neural Eng* 1: 63-71, 2004.

McCormick DA, and Bal T. Sleep and Arousal: Thalamocortical Mechanisms. *Annu Rev Neurosci* 20: 185-215, 1997.

McDonnall D, Clark GA, and Normann RA. Selective Motor Unit Recruitment Via Intrafascicular Multielectrode Stimulation. *Can J Physiol Pharmacol* 82: 599-609, 2004.

Menon V, Freeman WJ, Cutillo BA, Desmond JE, Ward MF, Bressler SL, Laxer KD, Barbaro N, and Gevins AS. Spatio-Temporal Correlations in Human Gamma Band Electrocorticograms. *Electroencephalogr Clin Neurophysiol* 98: 89-102, 1996.

Middlebrooks JC, and Snyder RL. Intraneural Stimulation for Auditory Prosthesis: Modiolar Trunk and Intracranial Stimulation Sites. *Hear Res* 242: 52-63, 2008.

Milekovic T, Fischer J, Pistohl T, Ruescher J, Schulze-Bonhage A, Aertsen A, Rickert J, Ball T, and Mehring C. An Online Brain-Machine Interface Using Decoding of Movement Direction from the Human Electrocorticogram. *J Neural Eng* 9: 046003, 2012.

Miller KJ, Hermes D, Honey CJ, Hebb AO, Ramsey NF, Knight RT, Ojemann JG, and Fetz EE. Human Motor Cortical Activity Is Selectively Phase-Entrained on Underlying Rhythms. *PLoS Comput Biol* 8: e1002655, 2012.

Miller KJ, Leuthardt EC, Schalk G, Rao RP, Anderson NR, Moran DW, Miller JW, and Ojemann JG. Spectral Changes in Cortical Surface Potentials During Motor Movement. *J Neurosci* 27: 2424-2432, 2007.

Miller KJ, Zanos S, Fetz EE, den Nijs M, and Ojemann JG. Decoupling the Cortical Power Spectrum Reveals Real-Time Representation of Individual Finger Movements in Humans. *J Neurosci* 29: 3132-3137, 2009.

Mitzdorf U. Current Source-Density Method and Application in Cat Cerebral Cortex: Investigation of Evoked Potentials and Eeg Phenomena. *Physiol Rev* 65: 37-100, 1985.

Mountcastle VB. An Organizing Principle for Cerebral Function: The Unit Module and the Distributed System. In: *The Mindful Brain*, edited by G. M. Edelman VBM. Massachusetts: MIT Press, 1978, p. pp. 7–50.

Nunez PL, and Srinivasan R. A Theoretical Basis for Standing and Traveling Brain Waves Measured with Human Eeg with Implications for an Integrated Consciousness. *Clin Neurophysiol* 117: 2424-2435, 2006.

Pfurtscheller G, Guger C, Muller G, Krausz G, and Neuper C. Brain Oscillations Control Hand Orthosis in a Tetraplegic. *Neurosci Lett* 292: 211-214, 2000.

Pistohl T, Ball T, Schulze-Bonhage A, Aertsen A, and Mehring C. Prediction of Arm Movement Trajectories from Ecog-Recordings in Humans. *J Neurosci Methods* 167: 105-114, 2008.

Pistohl T, Schmidt TS, Ball T, Schulze-Bonhage A, Aertsen A, and Mehring C. Grasp Detection from Human Ecog During Natural Reach-to-Grasp Movements. *PLoS One* 8: e54658, 2013.

Pistohl T, Schulze-Bonhage A, Aertsen A, Mehring C, and Ball T. Decoding Natural Grasp Types from Human Ecog. *Neuroimage* 59: 248-260, 2012.

Polikov VS, Tresco PA, and Reichert WM. Response of Brain Tissue to Chronically Implanted Neural Electrodes. *J Neurosci Methods* 148: 1-18, 2005.

Reimer J, and Hatsopoulos NG. Periodicity and Evoked Responses in Motor Cortex. *J Neurosci* 30: 11506-11515, 2010.

Rousche PJ, and Normann RA. Chronic Recording Capability of the Utah Intracortical Electrode Array in Cat Sensory Cortex. *J Neurosci Methods* 82: 1-15, 1998.

Sanchez JC, Gunduz A, Carney PR, and Principe JC. Extraction and Localization of Mesoscopic Motor Control Signals for Human Ecog Neuroprosthetics. *J Neurosci Methods* 167: 63-81, 2008.

Schalk G, McFarland DJ, Hinterberger T, Birbaumer N, and Wolpaw JR. Bci2000: A General-Purpose Brain-Computer Interface (Bci) System. *IEEE Trans Biomed Eng* 51: 1034-1043, 2004.

Schalk G, Miller KJ, Anderson NR, Wilson JA, Smyth MD, Ojemann JG, Moran DW, Wolpaw JR, and Leuthardt EC. Two-Dimensional Movement Control Using Electrocorticographic Signals in Humans. *J Neural Eng* 5: 75-84, 2008.

Schendel AA, Thongpang S, Brodnick SK, Richner TJ, Lindevig BD, Krugner-Higby L, and Williams JC. A Cranial Window Imaging Method for Monitoring Vascular Growth around Chronically Implanted Micro-Ecog Devices. *J Neurosci Methods* 218: 121-130, 2013.

Schevon CA, Goodman RR, McKhann G, Jr., and Emerson RG. Propagation of Epileptiform Activity on a Submillimeter Scale. *J Clin Neurophysiol* 27: 406-411, 2010.

Shushruth S, Davis T, Tasdizen T, Ichida J, House P, Greger B, and Angelucci A. Lfp Signals Evoked by Natural Image Stimulation of the Far-Surround of V1 Neurons Carry Contrast-Independent, Image-Specific Information. In: *Society for Neuroscience*. Washington, DC: 2011.

Slutzky MW, Jordan LR, Krieg T, Chen M, Mogul DJ, and Miller LE. Optimal Spacing of Surface Electrode Arrays for Brain-Machine Interface Applications. *J Neural Eng* 7: 26004, 2010.

Smith E, and Delargy M. Locked-in Syndrome. *BMJ* 330: 406-409, 2005.

Smith E, Kellis S, House P, and Greger B. Decoding Stimulus Identity from Multi-Unit Activity and Local Field Potentials Along the Ventral Auditory Stream in the Awake Primate: Implications for Cortical Neural Prostheses. *J Neural Eng* 10: 016010, 2013.

Solt K, and Forman SA. Correlating the Clinical Actions and Molecular Mechanisms of General Anesthetics. *Curr Opin Anaesthesiol* 20: 300-306, 2007.

Stacey WC, Kellis S, Patel PR, Greger B, and Butson CR. Signal Distortion from Microelectrodes in Clinical Eeg Acquisition Systems. *J Neural Eng* 9: 056007, 2012.

Tsanov M, Chah E, Wright N, Vann SD, Reilly R, Erichsen JT, Aggleton JP, and O'Mara SM. Oscillatory Entrainment of Thalamic Neurons by Theta Rhythm in Freely Moving Rats. *J Neurophysiol* 105: 4-17, 2011.

Turner JN, Shain W, Szarowski DH, Andersen M, Martins S, Isaacson M, and Craighead H. Cerebral Astrocyte Response to Micromachined Silicon Implants. *Exp Neurol* 156: 33-49, 1999.

Van Gompel JJ, Stead SM, Giannini C, Meyer FB, Marsh WR, Fountain T, So E, Cohen-Gadol A, Lee KH, and Worrell GA. Phase I Trial: Safety and Feasibility of Intracranial Electroencephalography Using Hybrid Subdural Electrodes Containing Macro- and Microelectrode Arrays. *Neurosurg Focus* 25: E23, 2008.

Velliste M, Perel S, Spalding MC, Whitford AS, and Schwartz AB. Cortical Control of a Prosthetic Arm for Self-Feeding. *Nature* 453: 1098-1101, 2008.

Velly LJ, Rey MF, Bruder NJ, Gouvitsos FA, Witjas T, Regis JM, Peragut JC, and Gouin FM. Differential Dynamic of Action on Cortical and Subcortical Structures of Anesthetic Agents During Induction of Anesthesia. *Anesthesiology* 107: 202-212, 2007.

Wang W, Collinger JL, Degenhart AD, Tyler-Kabara EC, Schwartz AB, Moran DW, Weber DJ, Wodlinger B, Vinjamuri RK, Ashmore RC, Kelly JW, and Boninger ML. An Electrocorticographic Brain Interface in an Individual with Tetraplegia. *PLoS One* 8: e55344, 2013.

Ward AA, and Thomas LB. The Electrical Activity of Single Units in the Cerebral Cortex of Man. *Electroencephalogr Clin Neurophysiol* 7: 135-136, 1955.

Warren DJ, Fernandez E, and Normann RA. High-Resolution Two-Dimensional Spatial Mapping of Cat Striate Cortex Using a 100-Microelectrode Array. *Neuroscience* 105: 19-31, 2001.

Waziri A, Schevon CA, Cappell J, Emerson RG, McKhann GM, 2nd, and Goodman RR. Initial Surgical Experience with a Dense Cortical Microarray in Epileptic Patients Undergoing Craniotomy for Subdural Electrode Implantation. *Neurosurgery* 64: 540-545; discussion 545, 2009.

Wolpaw JR, and McFarland DJ. Control of a Two-Dimensional Movement Signal by a Noninvasive Brain-Computer Interface in Humans. *Proc Natl Acad Sci U S A* 101: 17849-17854, 2004.

Worrell GA, Gardner AB, Stead SM, Hu S, Goerss S, Cascino GJ, Meyer FB, Marsh R, and Litt B. High-Frequency Oscillations in Human Temporal Lobe: Simultaneous Microwire and Clinical Macroelectrode Recordings. *Brain* 131: 928-937, 2008.

CHAPTER 2

THE EFFECTS OF PROPOFOL ON LOCAL FIELD POTENTIAL SPECTRA, ACTION POTENTIAL FIRING RATE, AND THEIR TEMPORAL RELATIONSHIP IN HUMANS AND FELINES[1]

2.1 Abstract

Propofol is an intravenous sedative hypnotic, which, acting as a $GABA_A$ agonist, results in neocortical inhibition. While propofol has been well studied at the molecular and clinical level, less is known about the effects of propofol at the level of individual neurons and local neocortical networks. We used Utah Electrode Arrays (UEAs) to investigate the effects of propofol anesthesia on action potentials (APs) and local field potentials (LFPs). UEAs were implanted into the neocortex of two humans and three felines. The two human patients and one feline received propofol by bolus injection, and the other two felines received target-controlled infusions. We examined the changes in LFP power spectra and AP firing at different levels of anesthesia. Increased propofol concentration correlated with decreased high-frequency power in LFP spectra and decreased AP firing rates, and the generation of large amplitude spike-like LFP activity; however, the temporal relationship between APs and LFPs remained relatively

[1] S. J. Hanrahan, B. Greger, R. A. Parker, T. Ogura, S. Obara, T. D. Egan, P. A. House, *Front. Hum. Neurosci*. Vol. 7:136 09 April 2013.

consistent at all levels of propofol. The probability that an AP would fire at this local minimum of the LFP increased with propofol administration. The propofol-induced suppression of neocortical network activity allowed LFPs to be dominated by low-frequency spike-like activity, and correlated with sedation and unconsciousness. As the low-frequency spike-like activity increased and the AP-LFP relationship became more predictable, firing rate encoding capacity was impaired. This suggests a mechanism for decreased information processing in the neocortex that accounts for propofol-induced unconsciousness.

2.2 Introduction

Propofol (2,6-di-isopropylphenol) is an intravenous sedative hypnotic and is an allosteric modulator of $GABA_A$ chloride channels. $GABA_A$ chloride channels are more densely located in the neocortex than in subcortical structures, and propofol therefore inhibits neural activity preferentially in the neocortex (Bai et al. 1999; Hentschke et al. 2005; Kaisti et al. 2002; Solt and Forman 2007). While the pharmacology and electroencephalography (EEG) effects of propofol have been extensively studied, its effects on action potentials (APs) and local field potentials (LFPs) are not yet well understood.

Most studies focusing on the electrophysiological effects of propofol have used low spatial resolution neural recording techniques, such as EEG and electrocorticography (ECoG). EEG investigations demonstrate that increasing propofol concentration in human subjects shifts cortical activity from a high-frequency, low-amplitude signal to a low-frequency, high-amplitude signal. Specifically, with increasing levels of propofol

anesthesia, beta activity (13 to 30 Hz) decreases and alpha (8 to 12 Hz) and delta activities (0.1 to 4 Hz) increase (Feshchenko et al. 2004). As propofol concentration is further increased, the EEG signal develops a burst suppression pattern with flat low-amplitude periods interspaced between high alpha and beta activity (Clark and Rosner 1973). At the highest levels of propofol sedation, the flat low-amplitude periods lengthen and the EEG signal becomes isoelectric (Claassen et al. 2002). Similar patterns have been seen by using intracranial ECoG recordings in human subjects during induction and emergence from propofol anesthesia. With the induction of anesthesia, delta band (1–2 Hz) power increases as gamma band (37–205 Hz) power decreases. In addition, the correlation between the phase of the delta band (1–4 Hz) and the power of the gamma band (23–165 Hz) strengthens with propofol anesthesia (Breshears et al. 2010).

Power in the high-frequency component of EEG signals corresponds to corticocortical activity (Gray and McCormick 1996), while power in the low-frequency component of EEG signals primarily arises from subcortical interactions (McCormick and Bal 1997). The decrease in high-frequency power with the administration of propofol may be due to a decrease in intracortical and corticocortical activity. The increase in low-frequency power may arise from interactions with subcortical structures such as the thalamus (Ching et al. 2010; Velly et al. 2007). Furthermore, the burst suppression pattern observed in the EEG signal in the anesthetized state is comparable with neural signal patterns seen in subcortical structures (Steriade et al. 1994). The activity in these subcortical structures may be observed in the neural signals throughout the cortex in the anesthetized state, resulting in an increased synchronization across the cortex (Steriade 2001).

In contrast to EEG and ECoG that integrate neural signals from large areas of cortex and are spatiotemporally smoothed, LFPs are recorded using high-impedance microscale electrodes and are thought to be generated by synaptic potentials (Katzner et al. 2009; Khawaja et al. 2009; Mitzdorf 1985; Nunez and Srinivasan 2006). While the spatial extent of LFPs is debated, they likely represent coordinated neural activity of cortical microcircuits, e.g., cortical columns. EEG and ECoG are unable to record APs from individual neurons or LFPs and are therefore unable to examine AP-LFP relationships (Buzsaki et al. 2012).

Arrays of microelectrodes can be used to examine the changes in LFP and AP activity during anesthesia. Utah Electrode Array (UEA) recordings in the rat cortex during the administration of urethane anesthesia demonstrated an overall decrease in AP firing and an increase in synchronous bursts of AP firing (Erchova et al. 2002). In addition, UEA recordings in the human cortex during the administration of propofol demonstrated a coupling between the slow (<1Hz) oscillation in the LFP and AP firing (Lewis et al. 2012). In this investigation, we examined the effects of propofol anesthesia on APs and LFPs and on the temporal relationship between these two neural signals. Two human patients and one feline were given propofol by bolus injection. A pharmacokinetic model was developed and was used for the target-controlled continuous infusion of propofol in two additional felines. Given that propofol reduces power in high frequencies and increases power in low frequencies in EEG and ECoG recordings, we hypothesized that similar effects would be seen on microelectrode recordings of APs and LFPs. In addition, the effect of propofol on the temporal relationship between APs and LFPs is unknown, and we aimed to determine whether propofol altered this relationship such that

information processing in the neocortex would be suppressed.

2.3 Methods

We used penetrating UEAs to investigate the electrophysiological changes resulting from propofol anesthesia at the level of single neuronal APs and LFPs. Each UEA (Blackrock Microsystems, Salt Lake City, UT) consisted of 96 electrodes, 1 mm in length, spaced 400 μm apart. UEAs were implanted into the cortices of two human patients and three felines. Reference electrodes for each UEA were placed in the subdural space greater than 2 cm away from the UEA. Neural activity was recorded and sampled at 30 kHz using a Cerebus system (Blackrock Microsystems). APs were identified using an automatic spike sorting algorithm (Shoham et al. 2003). The most prominent unit was used for each channel for consistency across all analysis. Neural activity was recorded at different sedation levels.

The study began with two humans (Patients A and B) given boluses of propofol. To evaluate whether the neurophysiological changes seen in the human could be replicated in an animal model under more controlled conditions, one feline (Feline A) was given boluses of propofol. To provide a controlled stepwise administration of propofol, a pharmacokinetic model was developed using a target-controlled infusion system for two additional felines (Felines B and C).

2.3.1 Human Studies

The two patients were enrolled in an Institutional Review Board–approved study. Each patient suffered from medically refractory temporal lobe epilepsy; on the basis of a

multidisciplinary review process, their condition was presumed to originate from the mesial temporal structures. We evaluated seizure semiology, routine EEG, video EEG, high-resolution MRI, and PET imaging.

In each case, a UEA was implanted in the middle temporal gyrus, approximately 3 cm from the temporal pole. The patients were maintained on a total intravenous anesthetic consisting of propofol and remifentanil during their craniotomy. Once the UEA was implanted, the anesthetic infusions were modulated to obtain a bispectral index scale (BIS) from a BIS Vista Monitoring System (Aspect Medical Systems, Norwood, MA) of ~50. The UEA made continuous recordings while boluses of propofol were administered intravenously to obtain a BIS of 20–30. The stable anesthetized state achieved before the boluses of propofol were delivered was considered baseline. For both patients, two rounds of BIS suppression with propofol boluses were recorded. The UEA was removed, and a standard anterior temporal lobectomy was then performed on each patient. Patient A (31-year-old man) underwent a right-sided resection, and Patient B (64-year-old man) underwent a left-sided resection. The hippocampus was histologically normal in each case. Specimens of lateral temporal neocortex from each patient contained thickening of the subpial plate, consistent with Chaslin's marginal sclerosis.

2.3.2 Feline Studies

In an Institutional Animal Care and Use Committee approved study, UEAs were implanted in the motor cortex of three felines. For Feline A, the neural activity was recorded continuously beginning while the feline was fully awake and continuing while it was given two boluses of propofol sufficient to mimic clinical burst suppression patterns

in the LFP. For felines B and C, a target-controlled infusion (TCI) system was developed to enable the achievement of pseudo steady-state propofol concentrations at or near a specified plasma level (Egan 2003). In brief, using raw propofol concentration versus time data obtained in a prior investigation (Bester 2009), the parameters for a three-compartment mammillary model were estimated using nonlinear regression techniques. This feline propofol pharmacokinetic model was then incorporated into Stanpump (Stanford University, Palo Alto, CA), a TCI software package that allows implementation of user-designated models. The TCI system was used to achieve and maintain predicted plasma propofol concentrations that were gradually raised over time. With the pharmacokinetic aspects of the experiment controlled in this manner, the pharmacodynamic measurements (i.e., electrophysiology and clinical observations) were made at each pseudo steady-state concentration plateau.

For Feline B, isoflurane was administered at the beginning of the experiment to place the intravenous catheter for propofol infusion. Propofol infusion started at a predicted plasma propofol concentration of 2 μg/ml for 10 minutes to allow time for elimination of isoflurane from the animal before the experiment began. For Feline C, the intravenous catheter was placed while the feline was fully awake and no isoflurane was administered. Eye blink, ear twitch, and toe pinch withdrawal reflexes were examined at each level of propofol infusion.

2.3.3 Analysis

For AP and LFP analysis, 30-second windows of data were examined during an awake (Feline A, B, and C) or baseline (Patient A and B) state, a lightly anesthetized

state (Patient A and B, Feline A, B, and C), a deeply anesthetized state (Patient A and B, Feline A, B, and C), and an isoelectric state (Feline C). The human patient data were all collected intraoperatively under a level of anesthesia appropriate for patient safety and comfort. Therefore, for these data, we will be referring to "lightly" and "deeply" anesthetized states only in a relative sense and only to simplify presentation. For the experiments in which propofol was delivered by bolus injection, clinical indicators of depth of anesthesia were not assessed as even the "light" state represents a clinical state consistent with general anesthesia. However, low-pass filtered (200 Hz) voltage traces can be used to categorize the 30-second time windows as belonging to the lightly or deeply anesthetized states by the resemblance of the voltage traces to the EEG waveforms from other human studies during their lightly and deeply anesthetized states, respectively (Brown et al. 2010). A low-pass filter of 200 Hz was applied to the voltage traces to closely approximate EEG waveforms seen in other human anesthesia studies.

The analyses of AP firing rate and LFP multitaper spectra were performed using the Chronux package (http://chronux.org) (Mitra and Bokil 2008). For LFPs, low-frequency bands are orders of magnitude larger in power than high-frequency bands (Miller et al. 2009). Therefore, each spectrogram was normalized by frequency bin to enhance visualization across the broad range of frequencies. Each time-frequency point was normalized by the minimum and maximum value of that frequency bin. LFP power in the high gamma band (60–120 Hz) was quantified over 30-second windows in three distinct brain states. The LFP power in the awake (felines) or minimally anesthetized (human patients) state was considered baseline, and the mean percent change from the LFP power in the awake state was calculated across all channels for each brain state. The

30-second periods of data were low-pass filtered at 200 Hz for each subject under varying levels of anesthesia. AP firing rate histogram was smoothed using a Gaussian kernel of 1-second and standard error bars were calculated using a bootstrapping procedure.

The temporal relationship of AP firing and LFP was examined by generating averaged AP-aligned LFP for three different levels of anesthesia. The time periods taken for the AP-aligned LFP analyses started at the same time as the 30-second windows for the awake or baseline state, lightly anesthetized state, and deeply anesthetized state. These time windows taken for analysis were extended by 3 minutes or longer to obtain enough APs. The temporal relationship between APs and the minimum value of the LFP during a 500-millisecond epoch around each AP was determined. A 500-millisecond epoch was chosen to capture the slowest AP-aligned LFP waveforms observed. Using epoch sizes of 200-milliseconds and 1000-milliseconds produced similar results because of the increased probability an AP would fire very close in time to the LFP minimum. The AP to minimum LFP value was created for each AP on all electrodes for the three different levels of anesthesia. A probability density function was created plotting the difference between the time the minimum value occurred in each LFP epoch and the time the AP fired. The integral of the probability density for the 50 milliseconds around the AP firing function yielded the probability that the minimum value of the LFP and AP firing occurred with 50 milliseconds of each other, i.e., they had a consistent temporal relationship. Randomly generated AP times were used to serve as a control in these analyses (Destexhe et al. 1999). The number of randomly generated APs was the same as observed in the original data to maintain AP firing rate. Randomly generated AP times were also used to generate averaged LFP epochs and served as a control for this analysis.

2.4 Results

All subjects, both human and feline, tolerated the experiments well. There were no adverse events relating to the propofol administrations. The human subjects enjoyed a routine postoperative course. Feline subjects were in good condition postexperiment. Increased propofol concentration resulted in suppression of small-amplitude, high-frequency activity and a dominance of large-amplitude, low-frequency spike-like activity in the LFP. For both patients, the LFP was initially a small-amplitude, high-frequency oscillatory signal in the baseline period (BIS = ~50). As the anesthesia was increased, the LFP developed into a larger-amplitude spike-like signal. In the deeply anesthetized state, the LFP consisted of large-amplitude spike-like activity separated by silent periods, which resemble EEG "bursts" (Figure 2.1A) (Table 2.1). We wished to evaluate whether the changes in LFP power seen in the human subjects could also be observed in an animal model under more controlled conditions, i.e., more disparate brain states and during steady states of anesthesia. In Feline A, continuous recordings were made from a fully awake state and two separate boluses of propofol were administered. During this feline model experiment, the observed changes in LFPs were similar to those observed in the human subjects (Table 2.1). To provide a controlled, stepwise administration of propofol, a pharmacokinetic model was developed using a TCI system for Felines B and C. During the controlled infusion of propofol, similar patterns of change in LFP power to those observed during bolus injections were observed. For Felines B and C, the LFP power in the high frequencies gradually decreased as the predicted propofol plasma concentration increased (Table 2.1). Additionally, the emergence from propofol hypnosis can be observed in the recordings as a return of power in the higher frequencies several

hundred seconds after bolus injection (Figure 2.1B) and as the target concentration of propofol was reduced (Figure 2.2).

The level of propofol correlated with the level of consciousness in both Felines B and C. Feline B in the lightly anesthetized state (predicted plasma propofol concentration = 6 µg/mL) made small voluntary movements and responded to touch. Eye blink, ear twitch, and toe pinch reflexes were still present at this level of anesthesia. In the deeply anesthetized state (predicted plasma propofol concentration = 8 µg/mL), only the eye blink reflex was present. For Feline B, an isoelectric state was not reached at the maximum level of anesthesia tested (predicted plasma propofol concentration of 18

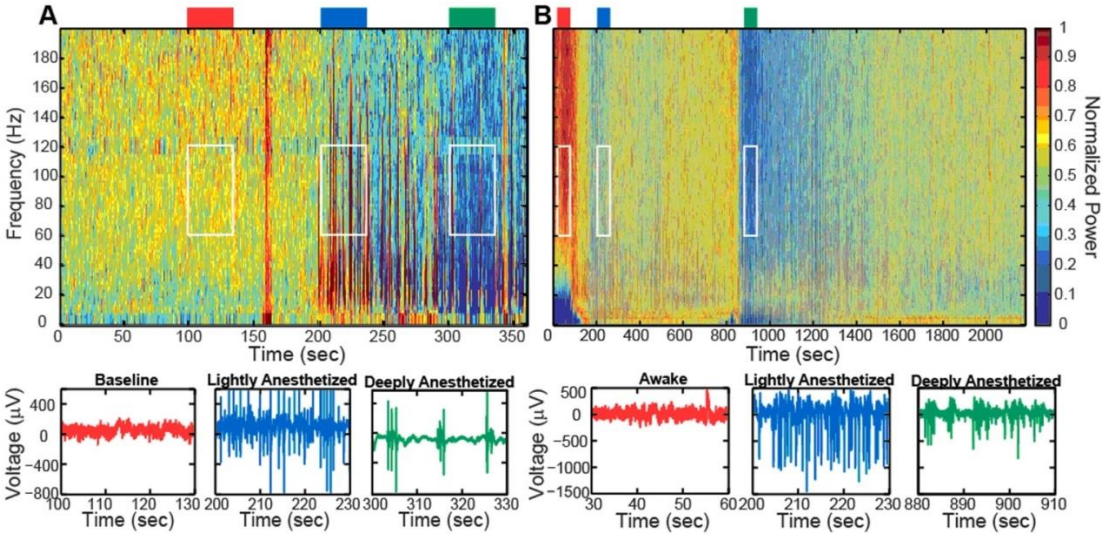

Figure 2.1. Boluses of propofol decreased the high-frequency power in the LFP spectra. Spectrogram and low-pass filtered traces (200 Hz) from one representative electrode for Patient A (A) and Feline A (B). Patient A received one bolus of propofol at ~200 s, while Feline A received two boluses of propofol at ~100 s and ~850 s. Colored rectangles above the spectrograms correspond with the level of anesthesia. Red represents the baseline or awake state. Blue represents the lightly anesthetized state. Green represents the deeply anesthetized state. White rectangles indicate the time periods and frequency bands chosen for the average power calculations across the array.

Table 2.1. Percent change in average power of a 30-second time window in the high gamma band (60–120 Hz) with respect to the baseline or awake state for all electrodes (N=96) (mean ± SD).

Subject	Lightly anesthetized (L)	Deeply Anesthetized (D)	Pairwise Significance
Patient A	16.01 ± 13.48 %	-28.67 ± 7.6 %	All pairs
Patient B	-4.96 ± 11.86 %	-10.09 ± 10.39 %	All pairs
Feline A	-29.79 ± 5.69 %	-41.35 ± 7.31 %	All pairs
Feline B	-20.22 ± 6.57 %	-22.69 ± 6.66 %	A/B-L, A/B-D
Feline C	-7.23 ± 3.38 %	-23.04 ± 2.84 %	All pairs

All changes in power were significant (Kruskal-Wallis, $p < 0.01$; multiple comparisons test, $p < 0.05$; A/B = Awake/Baseline, L = Lightly anesthetized, D = Deeply anesthetized).

µg/ml). Feline C in the lightly anesthetized state (predicted plasma propofol concentration = 8 µg/ml) made small voluntary movements and responded to touch. Eye blink, ear twitch, and toe pinch reflexes were still present at this level of anesthesia. In the deeply anesthetized state (predicted plasma propofol concentration = 14 µg/ml), the LFP developed bursts of large amplitude LFP separated by silent periods, i.e., burst suppression. Voluntary movement stopped, but eye blink, ear twitch, and toe pinch reflexes were present at this level of anesthesia. As anesthesia was increased, only the eye blink reflex remained at a predicted plasma propofol concentration of 18 µg/ml, and all reflexes were absent at a predicted plasma propofol concentration of 30 µg/ml. LFP power returned in the higher frequencies as the predicted plasma propofol concentration was decreased from 40 µg/ml (Figure 2.2).

In addition to altering the spectral power of LFPs, propofol administration also resulted in decreased AP firing rate. For Patients A and B, the average AP firing rate generally decreased across all electrodes in the array when comparing the baseline state

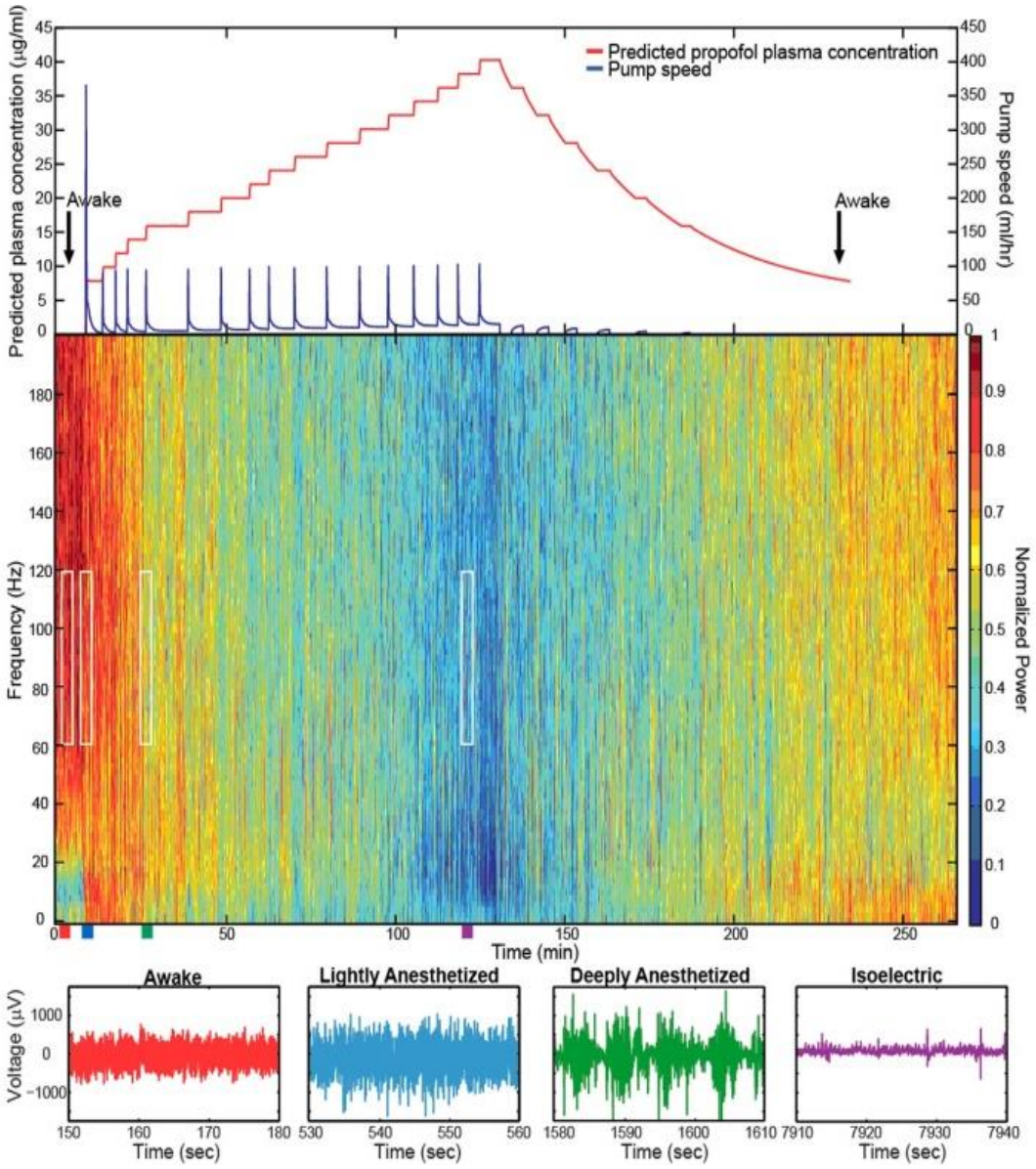

Figure 2.2. Target-controlled infusion of propofol gradually decreased the high-frequency power in the LFP spectra. Spectrogram and low-pass filtered traces (200 Hz) from one representative electrode in Feline C. Top plot show the predicted propofol plasma concentration using the target-controlled infusion system (red) and the TCI pump speed (blue) over the duration of the experiment. Induction and emergence from anesthesia occurred at nearly the same propofol concentrations as noted by the black arrows. Colored rectangles below the spectrogram correspond with the level of anesthesia. Red represents the awake state. Blue represents the lightly anesthetized state. Green represents the deeply anesthetized state. Purple represents the isoelectric state. White rectangles indicate the time periods and frequency bands chosen for the average power calculations across the array. With very high propofol concentrations, power in the LFP decreased across all frequency bands. After the peak propofol concentration is reached and the propofol concentration decreases, the power in the LFP increases.

with the lightly and deeply anesthetized states. For Feline A, the average AP firing rate decreased across all electrodes in the array comparing the awake state with the lightly and deeply anesthetized states. The recovery from the propofol boluses can be observed in the recording as return to higher AP firing rates over several hundred seconds after each bolus (Figure 2.3). The controlled infusion of propofol also yielded changes in AP firing rate similar to those observed during bolus injections. For Felines B and C, the average AP firing rates across the array gradually decreased as the predicted propofol plasma concentration increased (Table 2.2). For Feline C, APs in the isoelectric state were rare (predicted plasma propofol concentration = 40 μg/ml), but AP firing rates returned to higher levels as the propofol concentration was decreased (Figure 2.4).

Although AP firing rates and LFP activity were altered by anesthesia, AP-aligned LFP analysis demonstrated the temporal relationship between them remained relatively consistent across the different levels of anesthesia. The AP-aligned LFP exhibited a negative-going potential proximal in time to the APs. As the anesthesia increased, the AP-aligned LFP exhibited large-amplitude spike-like activity (Table 2.3). Because the number of well-isolated APs for Patient B was small, the AP-aligned LFP data from this subject was not analyzed. The phenomenon was also observed during the controlled infusion experiments. The LFP and AP temporal relationship was relatively consistent across all levels of anesthesia, i.e., APs fired during a local minimum in the LFP (Figure 2.5).

The probability that an AP would fire when the LFP reaches this local minimum increased with propofol administration. A probability density function was created plotting the difference between the time the minimum value occurred in each LFP epoch

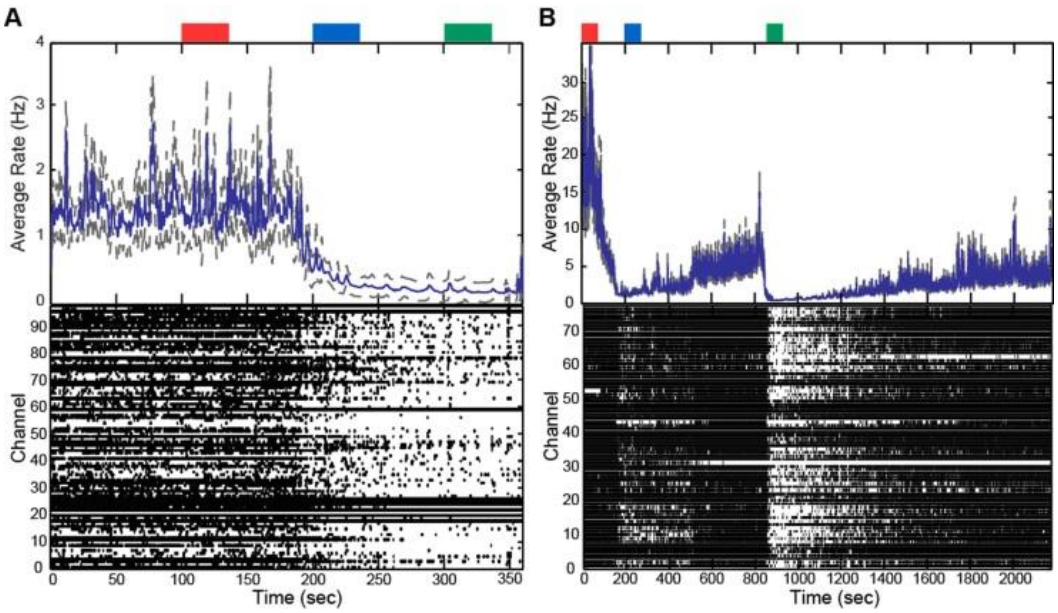

Figure 2.3. Boluses of propofol decreased firing rate across array. Raster plots and firing rate of Patient A (**A**) and Feline A (**B**). Patient A received one bolus of propofol at ~200 s, while Feline A received two boluses of propofol at ~100 s and ~850 s. Propofol boluses resulted in decreased AP firing rate as seen in the raster plots and firing rate histograms. The blue line represents the firing rate histogram and the gray dashed lines represent an interval of four standard errors wide centered at the mean. Colored rectangles above the plots correspond with time periods chosen for the average firing rate calculations. Red represents the baseline or awake state. Blue represents the lightly anesthetized state. Green represents the deeply anesthetized state. With the emergence from anesthesia, the firing rate begins to increase in Feline A after both boluses of propofol.

Table 2.2: Average firing rate for a 30-second time window for all subjects across all electrodes (N=96) (mean ± SD)

	Awake/Baseline (A/B)	Lightly Anesthetized (L)	Deeply Anesthetized (D)	Pairwise Significance
Patient A	1.426 Hz ± 1.912	0.4139 Hz ± 0.9779	0.1772 Hz ± 1.121	All pairs
Patient B	0.8781 Hz ± 0.9563	0.9014 Hz ± 0.9805	0.2208 Hz ± 0.3181	A/B-D L-D
Feline A	15.77 Hz ± 16.62	0.8125 Hz ± 0.8182	0.1663 Hz ± 0.2454	All pairs
Feline B	0.6538 Hz ± 2.107	0.0705 Hz ± 0.4123	0.0687 Hz ± 0.4518	A/B-L A/B-D
Feline C	0.3993 Hz ± 0.9782	0.150 Hz ± 0.3644	0.0257 Hz ± 0.0821	A/B-D

Values are mean ± SD.
All changes in firing rate were significant (Kruskal-Wallis, $p < 0.01$; multiple comparisons test, $p < 0.05$; A/B = Awake/Baseline, L = Lightly anesthetized, D = Deeply anesthetized).

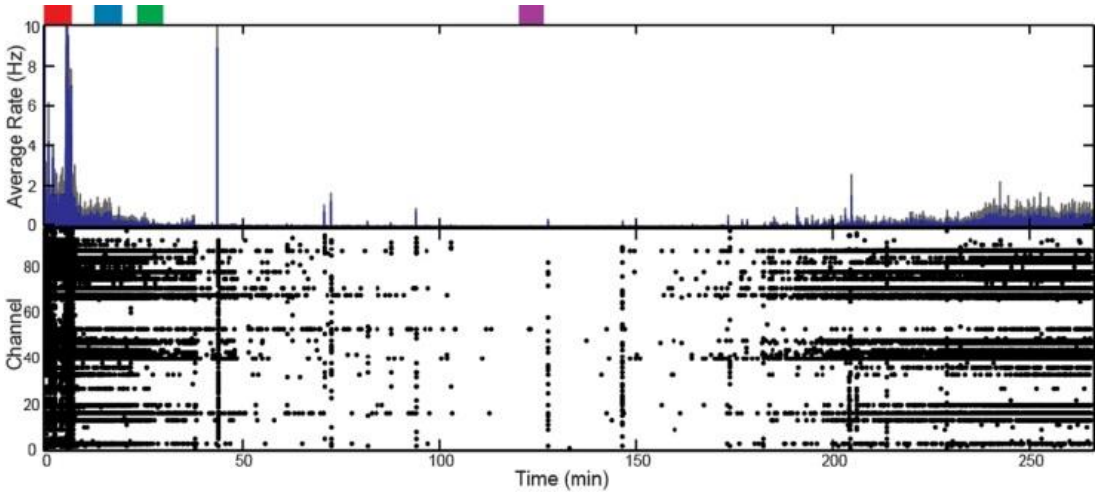

Figure 2.4. Target-controlled infusion of propofol decreased firing rate across the array for Feline C. Controlled infusion of propofol resulted in decreased AP firing rate as seen in the raster plot and firing rate histogram. The blue line represents the firing rate histogram and the gray dashed lines represent an interval of four standard errors wide centered at the mean. Colored rectangles above the plots correspond with time periods chosen for the average firing rate calculations. Red represents the awake state. Blue represents the lightly anesthetized state. Green represents the deeply anesthetized state. Purple represents the isoelectric state. With the emergence from anesthesia, the firing rate begins to increase 175 minutes into the recording.

Table 2.3: Average minimum across all electrodes (N=96) for the AP-aligned LFP analysis (mean ± SD)

	Awake/Baseline (A/B)	Lightly Anesthetized (L)	Deeply Anesthetized (D)	Pairwise Significance
Patient A	-23.16 μV ± 14.46	-217.22 μV ± 150.18	-204.96 μV ± 190.24	A/B-L A/B-D
Feline A	-47.28 μV ± 22.75	-354.90 μV ± 155.38	-280.02 μV ± 148.7	A/B-L A/B-D
Feline B	-133.36 μV ± 47.65	-766.16 μV ± 312.72	-615.28 μV ± 285.72	A/B-L A/B-D
Feline C	-141.93 μV ± 56.83	-582.29 μV ± 290.61	-577.45 μV ± 323.40	A/B-L A/B-D

All changes in power were significant (Kruskal-Wallis, $p < 0.01$; multiple comparisons test, $p < 0.05$; A/B = Awake/Baseline, L = Lightly anesthetized, D = Deeply anesthetized).

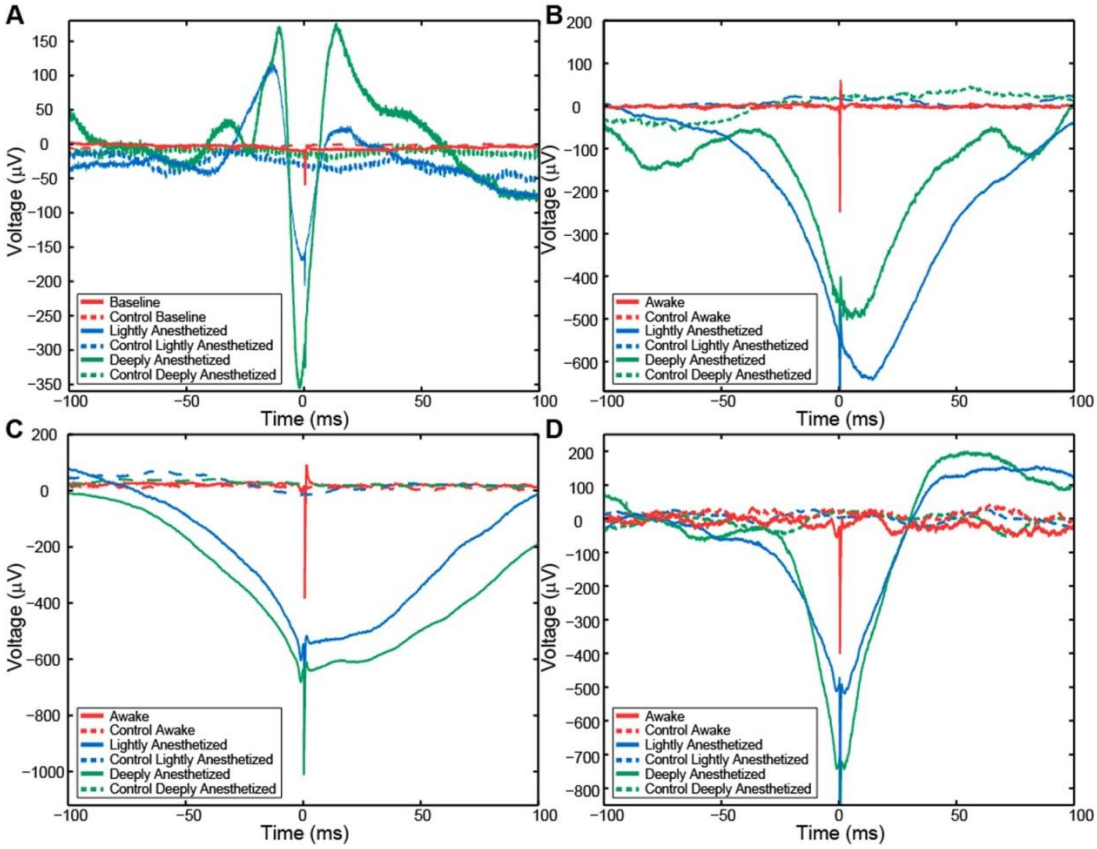

Figure 2.5. AP-aligned LFP plots for one representative channel from Patient A (**A**), Feline A (**B**), Feline B (**C**), and Feline C (**D**) in three distinct brain states. AP-aligned LFP exhibited a negative-going spike-like potential proximal in time to the APs. As the anesthesia increased, the amplitude of the spike-like LFP increased. Dashed lines represent the control cases in which randomly generate AP times were used to align the LFP. Red represents the awake state. Blue represents the lightly anesthetized state. Green represents the deeply anesthetized state.

and the time the AP fired. The integral of the probability density for the 50 milliseconds around the AP firing function yielded the probability that the minimum value of the LFP and AP firing occurred with 50 milliseconds of each other, i.e., they had a relatively consistent temporal relationship compared to control. Randomly generated AP times were used to generate averaged LFP epochs and served as a control for this analysis. For each subject, the probability that the minimum value of the LFP and AP firing had a consistent temporal relationship increased in the lightly and deeply anesthetized states from baseline (Figure 2.6) (Table 2.4).

2.5 Discussion

Previous studies of propofol in humans have used macroscopic EEG and ECoG electrodes, which integrate neural signals from large areas of the brain and cannot record APs from individual neurons. In the current study, UEAs were used to examine changes in high-frequency LFPs and in APs due to propofol administration in the human and feline. As hypothesized, increased propofol concentration decreased the high gamma (60–120 Hz) power in the LFP spectra and decreased AP firing rates in the neocortex. The temporal relationship between APs and LFPs remained relatively consistent across all levels of anesthesia, while the probability that an AP would fire when the LFP reach this local minimum increased from baseline with propofol administration. The changes in neural activity were correlated with decreased responsiveness, i.e., the level of consciousness.

In nonhuman primates, APs and LFPs were phase-locked in V4 during attention to visual stimuli (Fries et al. 2001), parietal cortex during activation of working memory

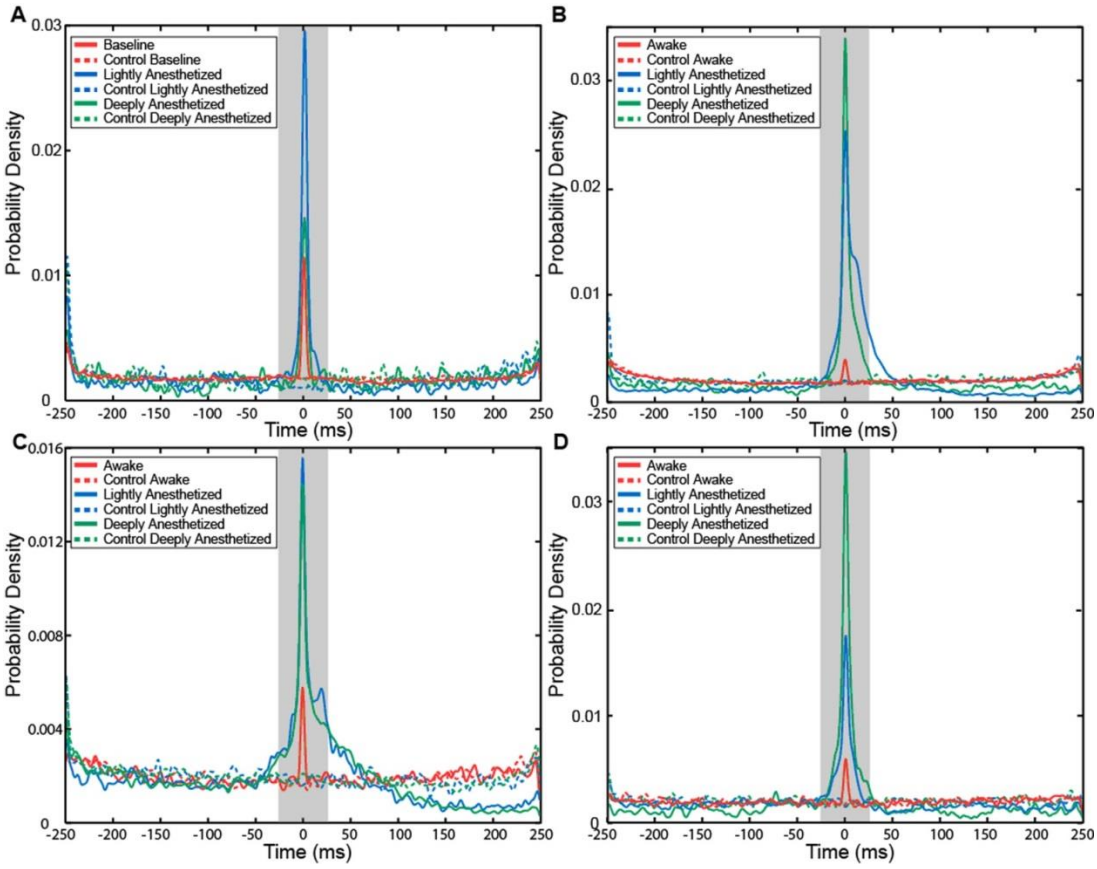

Figure 2.6. Probability density of the temporal separation between APs and the minimum LFP value for each AP on all electrodes for Patient A (A), Feline A (B), Feline B (C), and Feline C (D) at three different levels of anesthesia. The integral of the probability density for the 50 milliseconds around AP firing (shaded region) yielded the probability that the minimum value of the LFP and AP firing occurred with 50 milliseconds of each other, i.e., they had a consistent temporal relationship. With propofol administration, the probability of an AP occurring at the local minimum of the LFP increased. Dashed lines represent the control cases in which randomly generated AP times were used to align the LFP. Red represents the awake or baseline state. Blue represents the lightly anesthetized state. Green represents the deeply anesthetized state.

Table 2.4: Probability that a local minimum value of the LFP would occur within 50 ms of an AP for all electrodes

	Awake/ Baseline	Lightly Anesthetized	Deeply Anesthetized
Patient A	0.15 (0.09)	0.31 (0.06)	0.19 (0.08)
Feline A	0.10 (0.08)	0.48 (0.08)	0.40 (0.09)
Feline B	0.11 (0.08)	0.30 (0.09)	0.27 (0.09)
Feline C	0.11 (0.09)	0.27 (0.09)	0.45 (0.09)

Values in parentheses refer to control probabilities generated using random AP times.

(Pesaran et al. 2002), and motor cortex during voluntary movements (Donoghue et al. 1998). In human patients, APs and LFPs were observed to be phase-locked in the hippocampus, superior temporal gyrus, entorhinal cortex, orbitofrontal cortex, and amygdala (Jacobs et al. 2007). These nonhuman primate and human studies support that neurons represent information in terms of the timing of APs relative to neuronal oscillations.

We observed in the anesthetized states regularly occurring large-amplitude, spike-like potentials and burst suppression patterns replaced the small-amplitude, high-frequency oscillatory LFPs seen in the awake state, and AP firing was concomitantly decreased. However, the AP-LFP temporal relationship was maintained and the probability of an AP firing at the LFP local minimum was increased in the lightly and deeply anesthetized state compared to the awake and baseline states. A clear pattern of increasing probability not consistently seen between the lightly and deeply anesthetized states may be due to moderately high levels of anesthesia in the lightly anesthetized state. These anesthesia-induced changes in AP and LFP structure resulted in a decreased number of distinct neural activity patterns and therefore lowered the information capacity of the neural

signal (Alkire et al. 2008; Shannon and Weaver 1949). The entrainment of APs at low-frequency LFPs induced by propofol anesthesia would impair the amount of information represented in terms of the timing of APs relative to neuronal oscillations and decrease information processing of the cortex. Therefore, the effects of propofol anesthesia may be better characterized as a decrease in cortical information processing rather than as general neuronal inactivation.

That AP firing occurs when the transmembrane potential reaches a threshold voltage is well established (Hodgkin and Katz 1949); however, the relationship between the LFP and the transmembrane potential is less well understood. The transmembrane potential is the integration of the excitatory and inhibitory inputs onto a particular neuron, while the LFP represents the integration of the postsynaptic potentials from all neurons within several hundred micrometers of the recording electrode, i.e., the integration of the excitatory and inhibitory inputs to the local cortical circuitry. We did not observe that the probability of an AP occurring was related to a voltage threshold of the LFP; however, we observed that AP firing occurred with a high probability at a local minimum of the LFP. Across all levels of consciousness, AP firing was temporally correlated with the structure of the LFP, e.g., inflection points or minima, rather than a specific voltage level of the LFP. The occurrence of an inflection point in the LFP may reflect the moment that a significant shift occurs in the relative excitatory and inhibitory balance of the local network. $GABA_A$ inhibition induced by propofol alters the balance between excitatory and inhibitory activity in cortical circuits, and this altered balance is likely related to the observed changes in the LFP and the AP–LFP relationship. Simultaneous intracellular and extracellular recordings in awake rats using AP-aligned LFP demonstrated that the

LFP is correlated with the transmembrane depolarization of a single neuron (Okun et al. 2010). This finding, together with the consistently observed LFP–AP temporal relationship observed in the current study, suggest that there may be a biophysical mechanistic linkage between LFPs and APs. Many important neurophysiological animal studies are performed under various levels of hypnosis and anesthesia. Using intraperitoneal thiopental sodium to induce a lightly anesthetized state, and reduce AP firing due to top-down feedback and other processes, allowed the examination of AP firing in V1 driven by feedforward signals evoked by visual stimuli (Hubel and Wiesel 1959). Using a stimulus presentation paradigm that only allowed top-down feedback LFP signals to be recorded by electrodes in V1, it was possible to classify natural images based on decoding of the LFPs at above chance levels in the awake monkey, but only at chance levels in the anesthetized monkey (Shushruth et al. 2011). These studies show that varying the level of anesthesia can differentiate feedforward and feedback signals in V1. Similarly, studies examining AP–LFP relationships in V1 using AP-aligned LFP analysis achieved differing results under different levels of anesthesia. One study used awake monkeys (Ray and Maunsell 2011) and another used anesthetized monkeys and felines (Nauhaus et al. 2009). Intracortically recorded LFPs are thought to be generated by synaptic potentials (Katzner et al. 2009; Khawaja et al. 2009; Mitzdorf 1985; Nunez and Srinivasan 2006) that arise from multiple neural sources, and anesthesia can differentially alter the balance between these sources. Propofol binds to $GABA_A$ receptors that are located primarily in the cortex, so that propofol may impact corticocortical inputs more strongly than subcortical inputs. These studies and the present work demonstrate that while anesthetized preparations provide control of

experimental paradigms and are a powerful tool to dissect neurophysiological processes, the impact of the anesthesia itself on the neural system being studied must be taken into account when interpreting the results.

On the administration of propofol, we consistently observed a decrease in high-frequency power and AP firing rate, and an increase in regular and predictable patterns of LFP and AP activity. This reduced the information processing capacity in the neocortex and was correlated with a loss of responsiveness and consciousness. These effects of propofol on APs and LFPs have important implications for the processing of information in the neocortex, and therefore on the interpretation of experimental results in anesthetized preparations.

2.6 Acknowledgements

This work was supported by a Utah Research Foundation grant and DARPA BAA05-26 funding to BG. The authors thank Kristin Kraus for her editorial assistance, the CMC at the University of Utah for all their assistance in conducting the study, the EEG staff for assistance in conducting the study, and the patients for participating in the study.

2.7 References

Alkire MT, Hudetz AG, and Tononi G. Consciousness and Anesthesia. *Science* 322: 876-880, 2008.

Bai D, Pennefather PS, MacDonald JF, and Orser BA. The General Anesthetic Propofol Slows Deactivation and Desensitization of Gaba(a) Receptors. *J Neurosci* 19: 10635-10646, 1999.

Bester L. Pharmacokinetics of Propofol in Cats. In: *Companion Animal Clinical Studies*. Pretoria, South Africa: University of Pretoria, 2009, p. 61.

Breshears JD, Roland JL, Sharma M, Gaona CM, Freudenburg ZV, Tempelhoff R, Avidan MS, and Leuthardt EC. Stable and Dynamic Cortical Electrophysiology of Induction and Emergence with Propofol Anesthesia. *Proc Natl Acad Sci U S A* 107: 21170-21175, 2010.

Brown EN, Lydic R, and Schiff ND. General Anesthesia, Sleep, and Coma. *N Engl J Med* 363: 2638-2650, 2010.

Buzsaki G, Anastassiou CA, and Koch C. The Origin of Extracellular Fields and Currents--Eeg, Ecog, Lfp and Spikes. *Nat Rev Neurosci* 13: 407-420, 2012.

Ching S, Cimenser A, Purdon PL, Brown EN, and Kopell NJ. Thalamocortical Model for a Propofol-Induced Alpha-Rhythm Associated with Loss of Consciousness. *Proc Natl Acad Sci U S A* 107: 22665-22670, 2010.

Claassen J, Hirsch LJ, Emerson RG, and Mayer SA. Treatment of Refractory Status Epilepticus with Pentobarbital, Propofol, or Midazolam: A Systematic Review. *Epilepsia* 43: 146-153, 2002.

Clark DL, and Rosner BS. Neurophysiologic Effects of General Anesthetics. I. The Electroencephalogram and Sensory Evoked Responses in Man. *Anesthesiology* 38: 564-582, 1973.

Destexhe A, Contreras D, and Steriade M. Spatiotemporal Analysis of Local Field Potentials and Unit Discharges in Cat Cerebral Cortex During Natural Wake and Sleep States. *J Neurosci* 19: 4595-4608, 1999.

Donoghue JP, Sanes JN, Hatsopoulos NG, and Gaal G. Neural Discharge and Local Field Potential Oscillations in Primate Motor Cortex During Voluntary Movements. *J Neurophysiol* 79: 159-173, 1998.

Egan TD. Target-Controlled Drug Delivery: Progress toward an Intravenous "Vaporizer" and Automated Anesthetic Administration. *Anesthesiology* 99: 1214-1219, 2003.

Erchova IA, Lebedev MA, and Diamond ME. Somatosensory Cortical Neuronal Population Activity across States of Anaesthesia. *Eur J Neurosci* 15: 744-752, 2002.

Feshchenko VA, Veselis RA, and Reinsel RA. Propofol-Induced Alpha Rhythm. *Neuropsychobiology* 50: 257-266, 2004.

Fries P, Reynolds JH, Rorie AE, and Desimone R. Modulation of Oscillatory Neuronal Synchronization by Selective Visual Attention. *Science* 291: 1560-1563, 2001.

Gray CM, and McCormick DA. Chattering Cells: Superficial Pyramidal Neurons Contributing to the Generation of Synchronous Oscillations in the Visual Cortex. *Science* 274: 109-113, 1996.

Hentschke H, Schwarz C, and Antkowiak B. Neocortex Is the Major Target of Sedative Concentrations of Volatile Anaesthetics: Strong Depression of Firing Rates and Increase of Gabaa Receptor-Mediated Inhibition. *Eur J Neurosci* 21: 93-102, 2005.

Hodgkin AL, and Katz B. The Effect of Sodium Ions on the Electrical Activity of Giant Axon of the Squid. *J Physiol* 108: 37-77, 1949.

Hubel DH, and Wiesel TN. Receptive Fields of Single Neurones in the Cat's Striate Cortex. *J Physiol* 148: 574-591, 1959.

Jacobs J, Kahana MJ, Ekstrom AD, and Fried I. Brain Oscillations Control Timing of Single-Neuron Activity in Humans. *J Neurosci* 27: 3839-3844, 2007.

Kaisti KK, Metsahonkala L, Teras M, Oikonen V, Aalto S, Jaaskelainen S, Hinkka S, and Scheinin H. Effects of Surgical Levels of Propofol and Sevoflurane Anesthesia on Cerebral Blood Flow in Healthy Subjects Studied with Positron Emission Tomography. *Anesthesiology* 96: 1358-1370, 2002.

Katzner S, Nauhaus I, Benucci A, Bonin V, Ringach DL, and Carandini M. Local Origin of Field Potentials in Visual Cortex. *Neuron* 61: 35-41, 2009.

Khawaja FA, Tsui JM, and Pack CC. Pattern Motion Selectivity of Spiking Outputs and Local Field Potentials in Macaque Visual Cortex. *J Neurosci* 29: 13702-13709, 2009.

Lewis LD, Weiner VS, Mukamel EA, Donoghue JA, Eskandar EN, Madsen JR, Anderson WS, Hochberg LR, Cash SS, Brown EN, and Purdon PL. Rapid Fragmentation of Neuronal Networks at the Onset of Propofol-Induced Unconsciousness. *Proc Natl Acad Sci U S A* 109: E3377-3386, 2012.

McCormick DA, and Bal T. Sleep and Arousal: Thalamocortical Mechanisms. *Annu Rev Neurosci* 20: 185-215, 1997.

Miller KJ, Sorensen LB, Ojemann JG, and den Nijs M. Power-Law Scaling in the Brain Surface Electric Potential. *PLoS Comput Biol* 5: e1000609, 2009.

Mitra P, and Bokil H. *Observed Brain Dynamics*. Oxford ; New York: Oxford University Press, 2008, p. xxii, 381 p.

Mitzdorf U. Current Source-Density Method and Application in Cat Cerebral Cortex: Investigation of Evoked Potentials and Eeg Phenomena. *Physiol Rev* 65: 37-100, 1985.

Nauhaus I, Busse L, Carandini M, and Ringach DL. Stimulus Contrast Modulates Functional Connectivity in Visual Cortex. *Nat Neurosci* 12: 70-76, 2009.

Nunez PL, and Srinivasan R. A Theoretical Basis for Standing and Traveling Brain Waves Measured with Human Eeg with Implications for an Integrated Consciousness. *Clin Neurophysiol* 117: 2424-2435, 2006.

Okun M, Naim A, and Lampl I. The Subthreshold Relation between Cortical Local Field Potential and Neuronal Firing Unveiled by Intracellular Recordings in Awake Rats. *J Neurosci* 30: 4440-4448, 2010.

Pesaran B, Pezaris JS, Sahani M, Mitra PP, and Andersen RA. Temporal Structure in Neuronal Activity During Working Memory in Macaque Parietal Cortex. *Nat Neurosci* 5: 805-811, 2002.

Ray S, and Maunsell JH. Different Origins of Gamma Rhythm and High-Gamma Activity in Macaque Visual Cortex. *PLoS Biol* 9: e1000610, 2011.

Shannon CE, and Weaver W. *The Mathematical Theory of Communication*. Urbana,: University of Illinois Press, 1949, p. v (i.e. vii), 117 p.

Shoham S, Fellows MR, and Normann RA. Robust, Automatic Spike Sorting Using Mixtures of Multivariate T-Distributions. *J Neurosci Methods* 127: 111-122, 2003.

Shushruth S, Davis T, Tasdizen T, Ichida J, House P, Greger B, and Angelucci A. Lfp Signals Evoked by Natural Image Stimulation of the Far-Surround of V1 Neurons Carry Contrast-Independent, Image-Specific Information. In: *Society for Neuroscience*. Washington, DC: 2011.

Solt K, and Forman SA. Correlating the Clinical Actions and Molecular Mechanisms of General Anesthetics. *Curr Opin Anaesthesiol* 20: 300-306, 2007.

Steriade M. Impact of Network Activities on Neuronal Properties in Corticothalamic Systems. *J Neurophysiol* 86: 1-39, 2001.

Steriade M, Amzica F, and Contreras D. Cortical and Thalamic Cellular Correlates of Electroencephalographic Burst-Suppression. *Electroencephalogr Clin Neurophysiol* 90: 1-16, 1994.

Velly LJ, Rey MF, Bruder NJ, Gouvitsos FA, Witjas T, Regis JM, Peragut JC, and Gouin FM. Differential Dynamic of Action on Cortical and Subcortical Structures of Anesthetic Agents During Induction of Anesthesia. *Anesthesiology* 107: 202-212, 2007.

CHAPTER 3

DECODING ARTICULATE MOVEMENTS USING MICROSCALE SURFACE RECORDINGS IN HUMAN MOTOR CORTEX[2]

3.1 Abstract

Brain computer interfaces (BCIs) have the potential to help restore communication and motor functions to patients suffering from neurological disorders. By recording neural signals from the motor cortex, it may be possible to provide rapid and intuitive communication and prosthetic control. We demonstrated that speech, finger, and arm movements can be decoded from local field potentials (LFPs) recorded with dense grids of microelectrodes placed on the surface of human cerebral cortex. Five epilepsy patients who required long-term electrocorticographic (ECoG) monitoring were implanted with micro-ECoG grids. Patients were asked to perform specific tasks depending on the placement of the micro-ECoG grid on the cerebral cortex. Tasks included repeating spoken words, flexing individual fingers, and reaching in two dimensions. Using LFPs recorded over face-motor area, vocalized articulations of ten different words and silence were classified on a trial-by-trial basis with 82.4% accuracy.

---

[2] S. J. Hanrahan, S. Kellis, T. Davis, E. Smith, P.A. House, B. Greger.

Using LFPs recorded over the hand area of motor cortex, three individual finger movements and rest were classified on a trial-by-trial basis with 62% accuracy. LFPs recorded over the arm area of motor cortex were used to continuously decode the arm trajectory with a maximum correlation coefficient of 0.82 in the x-direction and 0.76 in the y-direction. These findings demonstrate that LFPs recorded by micro-ECoG grids from the surface of the cerebral cortex contain sufficient information to provide rapid and intuitive control a BCI communication system or motor prosthesis.

3.2 Introduction

Brain computer interfaces (BCIs) have the potential to help restore communication and motor function to patients suffering from neurological disorders. Amyotrophic lateral sclerosis (ALS) or spinal cord injury may leave patients severely paralyzed and unable to speak or interact with their environment in a condition known as locked-in syndrome (Smith and Delargy 2005). Some patients with locked-in syndrome depend on small residual movements for slow, basic communication and caregivers for physical interaction with their environment. By directly interfacing with the motor areas of the cortex, it may be possible to provide rapid and intuitive communication and prosthetic control (Birbaumer 2006). All such BCI systems transform neural activity related to intended movements into control signals for communication systems or assistive devices such as prosthetic arms. Ideally, the neural activity will be acquired with the highest spatial and temporal resolution possible, while using the most minimally invasive electrodes, in order to provide rapid, intuitive, and reliable control.

Researchers have a variety of electrode types to choose from when recording neural

activity from the cerebral cortex. Cortical activity related to movement can be recorded noninvasively from the scalp surface using electroencephalographic (EEG) electrodes. Studies have shown participants can use signals recorded with EEG to indirectly communicate by spelling words (Birbaumer et al. 1999; Schalk et al. 2004), move a computer cursor (Felton et al. 2009; Huang et al. 2009; Wolpaw and McFarland 2004), and provide 1-Dimensional control of a prosthetic arm (Hazrati and Erfanian 2010; Lauer et al. 1999; Pfurtscheller et al. 2000). EEG signals do not provide intuitive control of a prosthetic device because EEG records neural signals with prohibitively low temporal and spatial resolution.

Electrocorticography uses large (> 1 mm diameter) electrodes, typically placed beneath the dura, to map cortical function and locate an epileptic focus prior to the surgical treatment of epilepsy. Because ECoG is closer to the cortex, it can record neural signals with a higher signal-to-noise ratio and higher spatial resolution than EEG (Buzsaki et al. 2012; Cooper 1965). ECoG has become more common for BCI studies because of its clinical ubiquity in preparing patients for the surgical treatment of epilepsy. Neural activity recorded from ECoG electrodes has been used in the classification of spoken words or phonemes (Blakely et al. 2008; Chang et al. 2010; Leuthardt et al. 2004), classification of finger movements (Chestek et al. 2013; Kubanek et al. 2009; Miller et al. 2012; Miller et al. 2009; Pistohl et al. 2012) and the continuous decode of arm movement (Chao et al. 2010; Ganguly et al. 2009; Pistohl et al. 2008; Pistohl et al. 2013; Sanchez et al. 2008; Schalk et al. 2008). With many days of training, a patient with tetraplegia was able to control a prosthetic arm to perform limited reaching motions using cortical signals recorded over sensorimotor cortex with ECoG. The patient used

attempted movements of the thumb, elbow, and wrist to control the prosthetic arm (Wang et al. 2013). ECoG recordings in human motor cortex are limited to one or two electrodes modulating with movement (Leuthardt et al. 2004; Menon et al. 1996; Milekovic et al. 2012). Because of this, some ECoG studies use indirect, nonintuitive signals such as the movement of the tongue to control a computer cursor (Leuthardt et al. 2004; Schalk et al. 2008). ECoG electrodes are typically several millimeters in diameter with interelectrode spacing on the centimeter-scale. Therefore, ECoG grids spatially integrate and under-sample the information represented in the cerebral cortex at the scale of cortical columns.

Microelectrode arrays have the ability to record highly localized neural activity. Both surface and penetrating microelectrode arrays are able to record LFPs from a small population of neurons. LFPs recorded with high-impedance microelectrodes are thought to be generated by synaptic potentials (Katzner et al. 2009; Khawaja et al. 2009; Mitzdorf 1985; Nunez and Srinivasan 2006). While the spatial extent of LFPs is debated, they likely represent coordinated neural activity of cortical microcircuits, e.g., cortical columns (Buzsaki et al. 2012; Mountcastle 1978). High-impedance electrodes have a limited recording radius and record neural signals with minimal spatial integration (Tsanov et al. 2011). Therefore, microelectrode arrays can have smaller interelectrode spacing and avoid the issue of under-sampling cortical activity.

Patients with tetraplegia have participated in clinical trials with implanted penetrating microelectrode arrays. These arrays record action potentials (APs) from individual neurons in motor cortex and enable patients to control a computer cursor (Kim et al. 2011), and a prosthetic arm (Collinger et al. 2013; Hochberg et al. 2012). Due to an

increased risk of damaging eloquent cortex, few penetrating electrodes have been placed in the language areas of patients. One such study used a glass electrode filled with neurotrophic growth factor to encourage axonal growth into the electrode. The glass electrode was placed over the speech motor cortex to decode phonemes in real time (Guenther et al. 2009). Penetrating arrays are more invasive and AP recordings, which may last for years, do eventually degrade limiting the functional lifetime of these BCI systems (Barrese et al. 2013; Simeral et al. 2011). For BCI studies in which the penetrating microelectrode arrays were implanted for more than a year, AP sorting was hindered due to decreased AP amplitudes and threshold-crossing events were used to control 2-Dimensional movement (Chestek et al. 2011; Fraser et al. 2009).

Micro-ECoG grids were designed to record LFPs at high spatiotemporal resolution with an invasiveness equivalent to ECoG grids. Micro-ECoG electrodes have a small surface area, high impedance, and therefore record neural signals from a small volume of neural tissue. To avoid signal distortion, LFPs from micro-ECoG grids must be recorded by a high impedance amplifier (Stacey et al. 2012). Unlike penetrating microelectrode arrays, LFPs recorded from the surface of the cortex may be less prone to signal degradation over time (Schendel et al. 2013). The tighter interelectrode spacing of micro-ECoG grids provides the ability to sample the closely spaced areas of motor cortex that control different movement (Chestek et al. 2013; Crone 2006; Kim et al. 2007; Leuthardt et al. 2009; Menon et al. 1996; Miller et al. 2007; Slutzky et al. 2010; Van Gompel et al. 2008; Worrell et al. 2008). Micro-ECoG grids have shown promise for decoding speech (Kellis et al. 2010b; Leuthardt et al. 2011), arm movement (Kellis et al. 2009) and basic hand movements (Leuthardt et al. 2009). This work builds upon and

extends previous studies in which similar micro-ECoG grids have been shown to support high temporal- and spatial-resolution recordings for BCI-like applications (Kellis et al. 2012; Kellis et al. 2010b; Kellis et al. 2009).

We hypothesize that LFPs recorded on micro-ECoG grids can provide control signals for highly articulate prosthetic devices. To support this hypothesis, we used LFPs recorded with micro-ECoG grids placed over primary motor cortex to classify spoken word and individual finger movements, and to continuously decode the position of the hand during reaching.

3.3 Methods

3.3.1 Subjects and Grids

Data for this work were generated from human subjects in collaboration with the University of Utah, Department of Neurosurgery and under the approval of the Institutional Review Board. Human subjects were patients undergoing brain mapping procedures to identify the source of medication-resistant seizures.

Five patients were implanted with micro-ECoG grids (PMT Corporation, Chanhassen, MN and Ad-Tech Medical Instrument Corporation, Racine, WI; Table 3.1). Patients A and B were implanted with grids manufactured by PMT Corporation that consisted of 40 μm diameter platinum wire electrodes embedded in a thin layer of silicone. Each wire terminated in a cylindrical protuberance that extended approximately 200 μm above the base of the grid (Figure 3.1). Patient A was implanted with two 16 channel grids with 1 mm interelectrode spacing. Patient B was implanted with a 30 channel grid with 2 mm interelectrode spacing. Patients C, D, and E were implanted with

Table 3.1. Patient and grid information

	Sex	Task	Grid	Reference & Ground
Patient A	M	Speech Arm Movement	PMT Two 16 channels 40 μm, 1-mm spacing	Epidural wires
Patient B	M	Arm Movement	PMT 30 channels 40 μm, 2-mm spacing	On-grid low-impedance electrodes
Patient C	M	Finger Flexion Arm Movement Online Decode	Ad-Tech 64 channels 50 μm, 3-mm spacing	EEG electrodes
Patient D	M	Finger Flexion Arm Movement	Ad-Tech 32 channels 50 μm, 3-mm spacing	Nearest Subdural ECoG electrode EEG electrode
Patient E	F	Finger Flexion Arm Movement	Ad-Tech 32 channels 50 μm, 3-mm spacing	Nearest Subdural ECoG electrode Epidural ECoG electrode

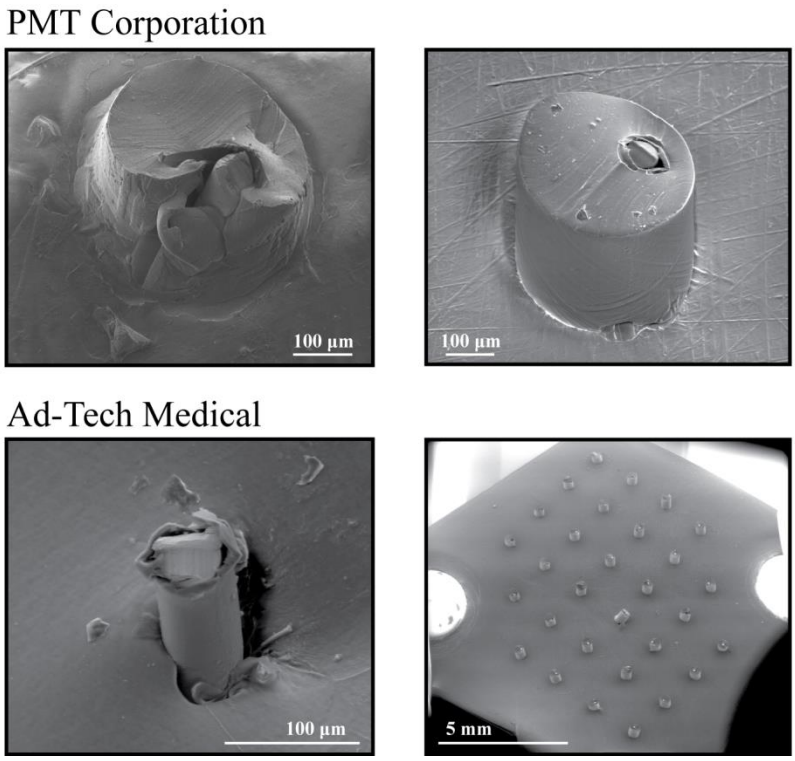

Figure 3.1. SEM pictures of micro-ECoG grids. Patients A and B were implanted with micro-ECoG grids manufactured by PMT Corporation. Each wire terminated in a cylindrical protuberance that extended ~200 µm above the base of the grid. Patients C, D, and E were implanted with micro-ECoG grids manufactured by Ad-Tech Medical. Each wire protruded above the base of the grid by ~80 µm.

grids manufactured by Ad-Tech Medical Instrument Corporation that consisted of 50 µm diameter platinum wire electrodes embedded in a thin layer of silicone. Each wire protruded above the base of the grid by approximately 80 µm. Patient C was implanted with a 64 channel grid and Patients D and E were implanted with 32 channel grids. The grids in Patients C, D, and E had 3-mm interelectrode spacing.

Clinical needs and constraints drove the placement of reference and ground. Ideally, reference and ground would be low-impedance electrodes located close to the micro-ECoG grids. For Patient A, reference and ground were low-impedance wires placed in the epidural space. For Patient B, reference and ground were on-grid low-impedance

ECoG electrodes. For Patient C, EEG electrodes located near the implantation site were used as reference and ground because all ECoG electrodes were necessary for clinical localization. To increase the quality of the EEG electrode reference and ground signals, a conductive gel was reapplied between the EEG electrodes and scalp prior to each experimental session. For Patient D, the reference was the nearest subdural ECoG electrode on the clinical grid and an EEG electrode was used for ground. For Patient E, the reference was the nearest subdural ECoG electrode on the clinical grid and ground was an epidural ECoG electrode (Table 3.1).

Micro-ECoG grids for all patients were implanted subdurally. As with the reference and ground, placement of the electrode grids was driven by clinical needs. In Patient A, the grids were initially implanted over the hand and arm representations of primary motor cortex. Patient A required a revision surgery to move the clinical ECoG grid and the two micro-ECoG grids were moved to be placed over face motor cortex and Wernicke's area during this surgery. The LFP recorded from face motor cortex classified words with a higher accuracy than the LFP recorded over Wernicke's (Kellis et al. 2010b). Therefore, the speech classification performed in this study only utilized data from the grid placed over face motor cortex. In Patients B – E, the grids were all implanted over the hand and arm representation in primary motor and somatosensory cortex (Table 3.1).

3.3.2 Experimental Paradigm

All behavioral and neural data were recorded with a NeuroPort system (Blackrock Microsystems, Salt Lake City, UT). A microphone recorded the patient's speech. Finger movement was monitored with three pressure sensors (Liberating Technologies,

Holliston, MA). To record the arm movement, patients used a computer mouse on a large tablet (Wacom, Vancouver, WA). A task control system (LabVIEW, National Instruments, Austin, TX) was used to visually cue patients.

For the speech task, the patient was verbally cued to repeat the words "Yes," "No," "Hot," "Cold," "Hungry," "Thirsty," "Hello," "Goodbye," "More," and "Less." For the finger task, patients were visually cued by the task control system to randomly flex their index, middle, and ring finger with the hand contralateral to the implanted electrodes. For the arm movement task, patients performed center out reaching movements after holding their arm at the start position for 500 ms with the arm contralateral to the implanted electrodes. Patients were verbally cued or visually cued using the task control system to move to random targets. Patients A and B experienced no hold times and Patients C, D, and E were instructed to hold their arm in the start position for 500 ms between cues. For the online Kalman filter decode, the task control system was also used to update the cursor position based solely on the Kalman filter estimate of position.

Patient A performed the speech task with multiple sessions over several days. Neural activity and speech were recorded at 30 kHz. Patients A and B performed the arm movement task and were verbally cued to the targets. The neural activity and computer cursor movement was sampled at 30 kHz. Patients C, D, and E performed both the finger flexion task and the arm movement task. The task control system was used to cue all movements. Neural data were recorded at 10 kHz and behavioral data were recorded at 2 kHz. Patient C had an additional online decode session in which he was instructed to move to two targets horizontally separated. Neural and hand position data were down sampled to 5 kHz (Patient A) or 2 kHz (Patients B, C, D, and E) to reduce data size for

analysis. The neural data were also high-pass filtered at 1 Hz to attenuate motion artifact (Table 3.1).

3.3.3 Data Analysis

Data from each microelectrode were re-referenced by subtracting the common average across 16 channel blocks of electrodes, which were located within close proximity. All LFPs were visually inspected by plotting low-pass filtered (200 Hz) voltage time series of representative electrodes to identify excessive noise. Several channels had high 60 Hz noise. Channels were excluded if the average power between 59 to 61 Hz was greater than twice the average power of the broadband signal. For the remaining channels, 60 Hz and its harmonics were excluded from the data using a comb filter.

3.3.3.1 Speech Classification

For speech classification, different types of LFP features were selected as the decode input to explore dynamics in the time domain as well as the frequency domain. To examine the time domain, the voltage time series of all channels was downsampled to 100 Hz. The voltage time series was also normalized across trials for each channel. To examine the frequency domain, the power spectra for all channels were estimated for frequencies between 1-1000 Hz. LFP multitaper spectra were generated using the Chronux package (http://chronux.org) (Mitra and Bokil 2008) and were log-normalized across trials for each channel. The frequency domain consisted of one vector of power in different frequency bands for each trial for each channel. Frequencies between 1 and

1000 Hz were chosen because the spectrogram of the raw data showed increased power with each word throughout this frequency band. The time domain LFP features were constrained in time from the 0.25 seconds before the onset of articulation to 0.5 seconds after. The frequency domain LFP features were constrained in time from the onset of articulation to 0.5 seconds. A baseline period was used to represent a silence state when the patient was not speaking. The LFP features for the baseline period were calculated using data from the 1 second to 0.25 seconds before the onset of articulation for the time domain and 0.75 seconds to 0.25 seconds before the onset of articulation for the frequency domain.

Speech classification was performed on the time domain features and the frequency domain features separately and in combination (Figure 3.2). PCA was performed on LFP features collected from 30 training trials for each word to decorrelate the data. A number of leading principal components sufficient to preserve 90% of the variance in the data were used in the decode. During the decode phase, projected feature vectors from 20 subsequent testing trials for each word were classified using linear discriminant analysis. For Patient A, ten words and a baseline period were classified.

3.3.3.2 Finger Flexion Classification

For finger flexion classification, different types of LFP features were selected as the decode input to explore dynamics in the time domain as well as the time varying frequency domain. To examine the time domain, the voltage time series of all channels was downsampled to 100 Hz. The voltage time series was also normalized across trials for each channel. To examine the time varying power in the frequency domain, the

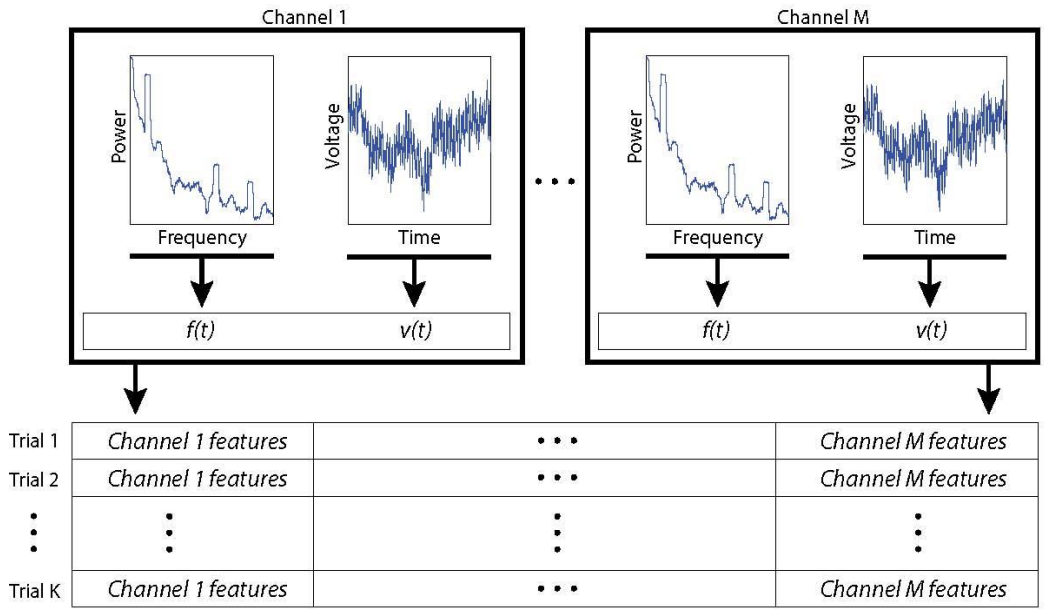

Figure 3.2. Using features from time and frequency domain from multiple channels for the classification of spoken words and finger movements. Power spectra were calculated for each trial and each microelectrode, and were concatenated with down sampled voltage time series. Trials were stacked to form a large 2-dimensional matrix of microelectrode and trial information. The same number of principal components was retained for each case. The selected features capture relevant dynamics in time, space, and frequency.

power spectra for all channels were estimated for frequencies between 65 and 115 Hz each 100 ms time bin. LFP multitaper spectra were generated using the Chronux package and were log-normalized across trials for each channel. Spectra were calculated over 100 ms time bins, forming vectors of power in different frequency bands that were stacked to build a matrix of time varying frequency features. Frequencies between 65 and 115 Hz were chosen because it reflects the high gamma and low chi bands that has been shown to modulate with finger movement (Chestek et al. 2013). The LFP features were constrained in time from the 200 ms before the onset of movement to 1000 ms after. A baseline period was used to classify a rest state when there was no finger movement. The baseline period was calculated using data from the 1200 ms before the onset of the cue to

the onset of cue.

Finger flexion classification was performed on the time domain features and the time varying frequency domain features separately and in combination (Figure 3.2). PCA was performed on LFP features collected from training trials for each movement type to decorrelate the data. A sufficient number of leading principal components were retained to preserve 90% of the variance in the data. During the decode phase, projected feature-vectors from subsequent testing trials for each movement type were classified using linear discriminant analysis. For Patient C, LFP features from 64 channels were used for 40 training trials and 40 testing trials. For Patient D, LFP features from 26 channels were used for 30 training trials and 19 testing trials. For Patient E, LFP features from 30 channels were used for 40 training trials and 40 testing trials.

3.3.3.3 Continuous Decode of Arm Movement

For the continuous decode of arm movement, different types of LFP features were selected as the decode input to explore dynamics in the time domain as well as the time varying power in the frequency domain. To examine the time domain, the voltage time series was averaged for each 100 ms time bin. LFP multitaper spectra were generated using the Chronux package and were log-normalized across trials for each channel. To examine the time varying frequency domain, the spectral power at 1-5 Hz, 10-15 Hz, 25-30 Hz, 50-55 Hz, 100-105 Hz, and 250-255 Hz was estimated for each 100 ms time bin. Frequency bands were chosen because the spectrogram of the raw data showed increased power with arm movement distributed between 1-255 Hz.

To continuously decode arm movement, a standard Kalman filter was implemented.

The likelihood model was defined as

$$z_k = H_k x_k + Q_k \quad (1)$$

where H_k linearly relates the arm kinematics x_k to the LFP features z_k. Q_k represents noise in the observation, assumed to be zero-mean and normally distributed. The final feature vector $z_k$consisted of LFP features for each channel.

$$x_{k+1} = A_k x_k + W_k \quad (2)$$

The state transformation matrix A_k was defined to model how the arm kinematics, varied over time, with W_k, a noise term, also assumed to be zero-mean and normally distributed. The arm kinematic state x_k comprised x and y position, velocity, and acceleration for k = 1, 2, ... M, where M was the number of time bins in the data set. The parameters A, H, W, and Q were directly calculated from the training data as described in (Wu et al. 2006) and were assumed to be constant, e.g., $A_k = A$..

The LFP and arm kinematic data were segmented into 100 ms time bins and the decode updated the estimated position each 100 ms time bin. The Kalman filter was performed with $z_k$as the time domain features and the time varying frequency domain features separately and in combination. An offset of 200 ms was introduced between the movement data and the LFP feature set to account for the delay between neural activity and motor output. The Kalman filter was trained and then tested on subsequent nonoverlapping segments of data.

For Patient A, the LFP features were selected from 32 channels. The training set was

112 seconds (31 reaches) and the testing set was the subsequent 89 seconds (25 reaches) after 225 seconds of the patient resting. For Patient B, the LFP features were selected from 30 channels. The training set was 55 seconds (19 reaches) and) and the testing set was the subsequent 65 seconds (28 reaches) after 15 seconds had passed. For Patient C, the LFP features were selected from 64 channels. The training set was 180 seconds (70 reaches) and the testing set was the subsequent 180 seconds (68 reaches). For Patient D, LFP features were selected from 26 of the 32 channels. The training set was 180 seconds (52 reaches) and the testing set was the subsequent 120 seconds (36 reaches). For Patient E, LFP features were selected from 32 channels. The training set was 120 seconds (20 reaches) and the testing set was the subsequent 120 seconds (25 reaches).

For Patient C, the Kalman filter was also implemented online in real-time. LFP and kinematic data were segmented into 100 ms time bins, with an offset of 200 ms between neural data and kinematics. Eighteen channels were selected for the decode. These channels were chosen because the LFPs demonstrated the highest correlation coefficients with arm movement. For the selected channels, spectral data in the beta band, 20 to 30 Hz, were averaged. The beta band was selected because there was a visual increase in power between 20 to 30 Hz when the patient made reaching movements. For other studies decoding arm movement, power in frequencies above 100 Hz has been shown to have higher mutual information with kinematic data, but power in the beta band had a moderate value of mutual information with the kinematic data (Zhuang et al. 2010). The decode was trained using 1 minute of data. The position of the cursor during online decoding was restricted within the space of the tablet and monitor, but no algorithmic constraints were applied to trajectory. Patient C received visual feedback while the task

control system updated the cursor position based on the Kalman filter output every 100 ms. A trial was considered successful immediately after the patient crossed the perimeter of the 50 mm diameter target. The target remained on until the trail was successful.

3.3.4 Evaluation

Classification accuracy was measured against the level of chance, which was determined by assuming a uniform distribution for each class assignment. Classification accuracies above the level of chance indicates that the LFP features applied to the classification were correlated to the behavior measured. Confusion matrices were also computed for classification decodes. Each value on a given row and column of a confusion matrix represents the normalized number of times that a class was predicted by the decoder. If the decoding is perfect, the confusion matrix should be an identity matrix, i.e., have entries equal to one along the main diagonal and zero everywhere else.

To determine the level of chance in the context of the continuous trajectory decode, the Kalman filter was trained and tested using a LFP feature set in which the 0.1 second time bins were randomized. Recorded kinematic data were maintained. The Kalman filter was performed for all five patients using the randomized time and frequency domain feature sets. The correlation coefficients for each kinematic variable were averaged across the five patients to obtain the level of chance values.

3.4 Results

3.4.1 Speech Classification

For speech classification, combining features from the time and frequency domain improved performance relative to using only the time domain or frequency domain features. Using LFP features from only the time domain, two words were classified with a median accuracy of 93.3% and eleven words were classified with an accuracy of 67.9%. Using LFP features from only the frequency domain, two words were classified with a median accuracy of 96.7% and eleven words were classified with an accuracy of 49.7%. However, when using LFP features from both the time and frequency domains, the greatest accuracy was achieved with two words classified with a median accuracy of 99.9% and 11 classes (10 words and silence) classified with an accuracy of 82.4%. In all cases, the median accuracy for all combinations of words was classified well above chance of 50% for two words and 9.1% for eleven words (Figure 3.3A). The confusion matrix shows the number of times each word or silence was predicted by the decoder using features from the frequency and time domain (Figure 3.3B). Periods of silence in which the patient was not speaking was classified with the highest accuracy. Words such as “no” and “less” were classified more accurately than words such as “hello” and “cold.”

3.4.2 Finger Flexion Classification

For finger flexion classification, combining features from the time and frequency domain also improved performance relative to using only the time domain or frequency domain features. For Patient D, using LFP features from only the time domain, two finger movements were classified with a median accuracy of 71.1% and four finger

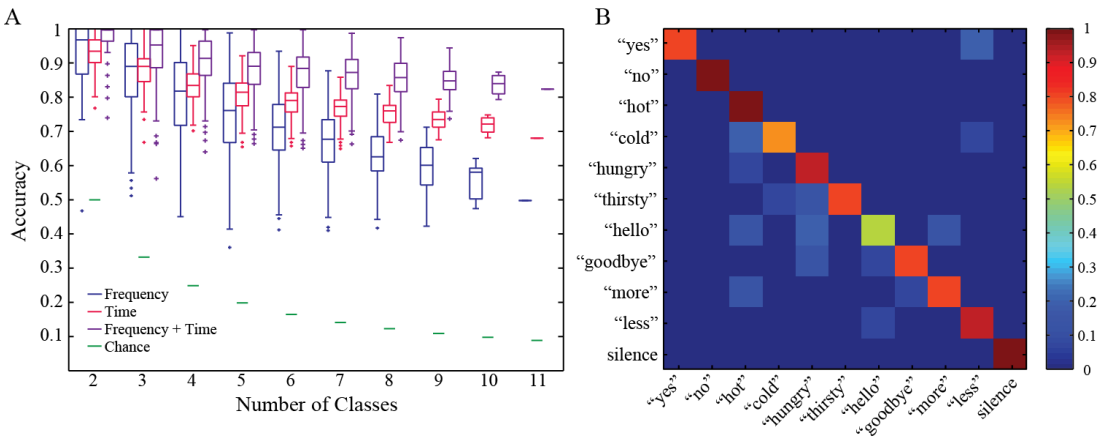

Figure 3.3. Comparing performance of classification of speech for two through eleven words simultaneously classified for Patient A. (A) Performance of speech classification for two to ten words and silence using only frequency domain features, only time domain features, and with combined time and frequency domain features from LFP recorded over face motor cortex. (B) Confusion matrix showing the number of times each word or silence was predicted by the decoder using the combined time and frequency domain features.

movements were classified with an accuracy of 40.8%. Using LFP features from only the frequency domain, two finger movements were classified with a median accuracy of 77.6% and four finger movements were classified with an accuracy of 56.6%. When using LFP features from both the time and frequency domains, the greatest accuracy was achieved with two finger movements classified with a median accuracy of 77.6% and four finger movements classified with an accuracy of 61.8% (Figure 3.4A). For Patient C, the accuracy for four finger movements was 46.4% using only time domain features, 50.3% using only frequency domain features, and 53% using both time and frequency domain features. For Patient E, the accuracy for four finger movements was 30% using only time domain features, 28.8% using only frequency domain features, and 38.3% using both time and frequency domain features. The median accuracy for all combinations of finger movements was classified well above the chance level of 25%. The confusion matrix in Figure 3.4B shows the number of times each movement was

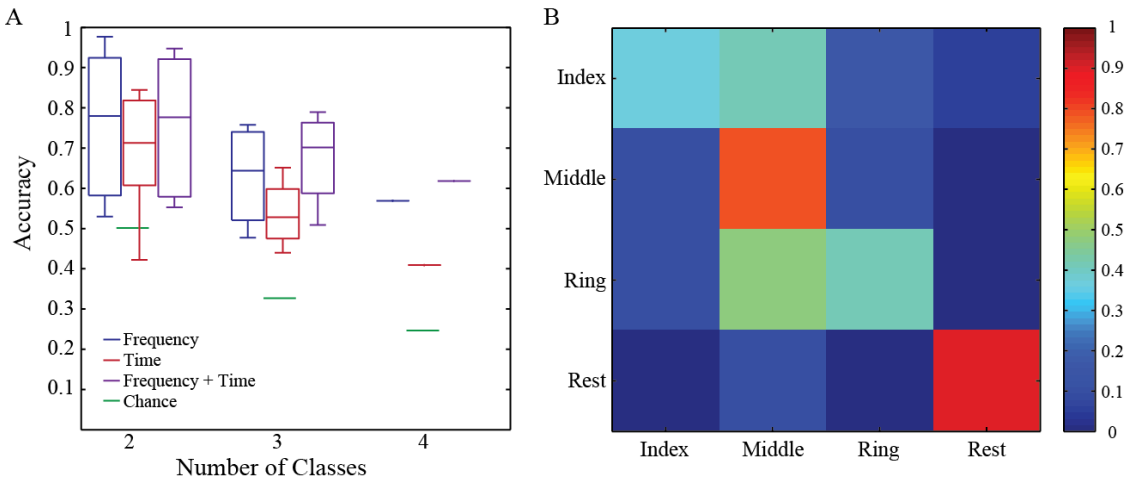

Figure 3.4. Comparing performance of classification of speech for two through four finger movements simultaneously classified for Patient D. (A) Performance of finger flexion classification for two to three finger movements and rest using only frequency domain features, only time domain features, and with combined time and frequency domain features. (B) Confusion matrix showing the number of times each finger movement or rest was predicted by the decoder using the combined time and frequency domain features. Perfect classification would be a dark red diagonal line.

predicted by the decoder using features from the frequency and time domain for Patient D. Rest and middle finger flexion was more accurately classified than index and ring finger flexion.

3.4.3 Continuous arm movement decode

For the continuous decode of arm movement, the performance of the decode was quantified offline by calculating the correlation coefficient between the actual arm position, velocity, and acceleration and the estimated arm position, velocity, and acceleration. Applying LFP features from both the time and frequency domain, the Kalman filter decode was able to estimate the arm movements for Patient B with the highest correlation (Figure 3.5). The estimated position and the actual position of the arm had correlation coefficients of 0.82 in the X direction and 0.76 in the Y direction. The

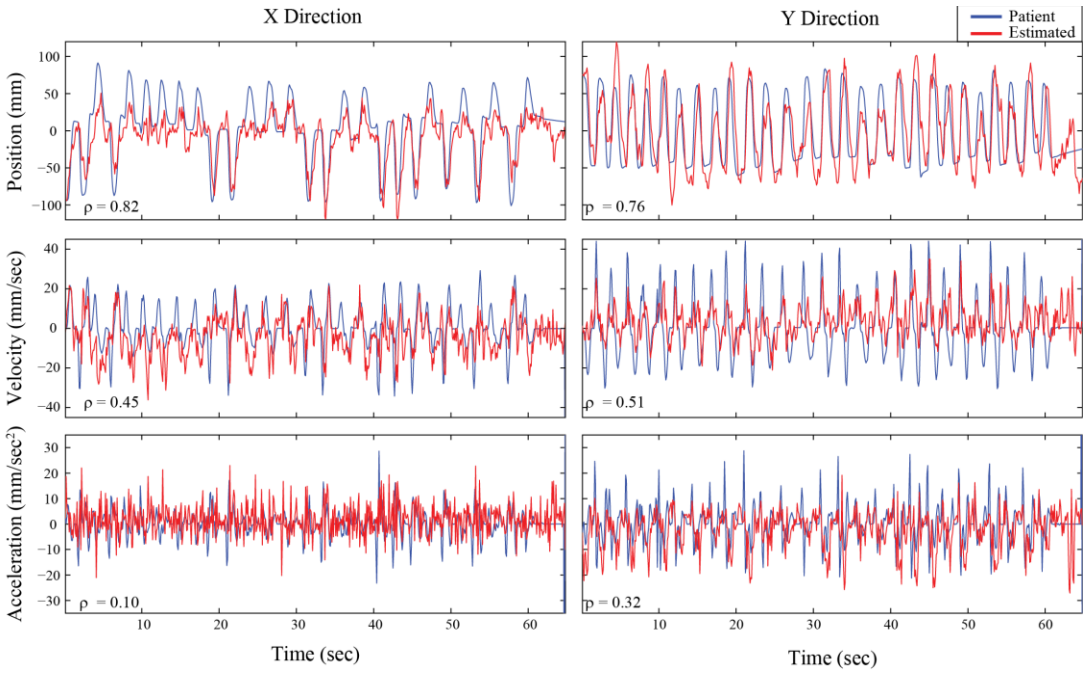

Figure 3.5. Output of the Kalman filter decode for Patient B. Comparison of actual X and Y arm kinematics (blue) to estimated X and Y arm kinematics (red) of the computer cursor during a 2-Dimensional task. The Kalman filter was performed on 30 channels using LFP features from both the time and frequency domain. A lag time of 0.2 sec was added to the LFP feature set. The Kalman filter was trained on 55 seconds of data and tested on 65 seconds of data.

estimated velocity and the actual velocity of the arm had correlation coefficients of 0.45 in the X direction and 0.51 in the Y direction. The estimated acceleration and the actual acceleration of the arm had correlation coefficients of 0.10 in the X direction and 0.32 in the Y direction. Using LFP features from the time and frequency domain, the decode performed well above chance for X and Y position, velocity, and acceleration for all patients (Table 3.2). The correlation coefficients between the actual and estimated kinematic variables were averaged together in order to compared decode performance for the three possible LFP feature sets (time, frequency, and time+frequency). Combining features from the time and frequency domain improved performance slightly from using only the time domain or frequency domain features (Table 3.2). The decode had the

Table 3.2. Correlation coefficients between actual and estimated arm kinematics for all patients

	Patient A	Patient B	Patient C	Patient D	Patient E	Chance
X Position	0.32	0.82	0.66	0.53	0.35	0.10
Y Position	0.39	0.76	0.54	0.45	0.25	0.12
X Velocity	0.17	0.45	0.43	0.39	0.30	0.09
Y Velocity	0.32	0.51	0.36	0.36	0.16	0.05
X Acceleration	0.12	0.10	0.40	0.19	0.16	0.03
Y Acceleration	0.20	0.32	0.21	0.08	0.10	0.03
Average (time + frequency domain)	0.25	0.49	0.43	0.33	0.22	0.07
Average (time domain)	0.18	0.31	0.41	0.24	0.13	0.07
Average (frequency domain)	0.24	0.39	0.32	0.24	0.16	0.07

lowest correlation coefficients for Patients A and E, which may be due to a less ideal positioning of the grid over the arm area of cortex or decreased contact with the cortex.

For the online experiment, Patient C neurally controlled the movement of a computer cursor using the real-time Kalman filter. The patient moved the cursor between two targets, which were visually cued for 21 minutes (Figure 3.6). The patient required a median of 2.15 seconds (Interquartile Range of 3.78) to start moving in the direction of the target, and a median of 6.24 seconds (Interquartile Range of 14.29) to acquire each target. All presented targets were successfully reached because the target remained on until the patient reached the perimeter of the target for a successful trial.

3.5 Discussion

We hypothesized that micro-ECoG grids could acquire neural signals with high spatial and temporal resolution from the primary motor cortex of human patients. If so,

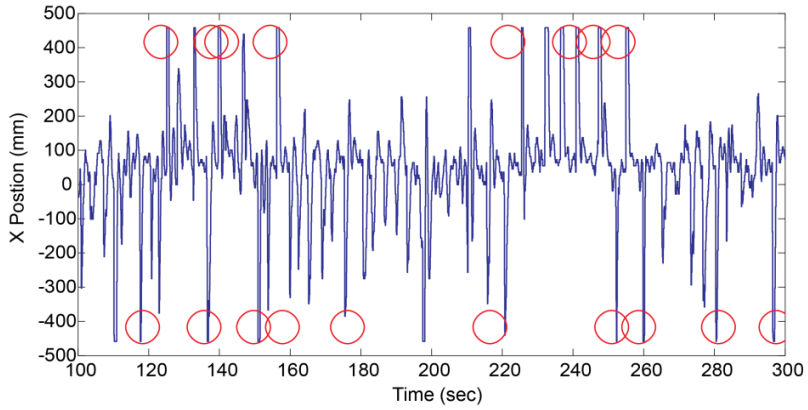

Figure 3.6. X position of a computer cursor neurally controlled by Patient C with a real-time Kalman filter decode. A 300-second representative sample of performance of the real-time Kalman filter decode is shown. The blue line represents the x position in millimeters of the cursor as Patient C was randomly cued to move to two targets (red circles) horizontally separated on the monitor. A single feature was used from 18 channels, consisting of the average power between 20 and 30 Hz. The real-time Kalman filter was trained on 60 seconds of data and was implemented with 100 ms time bins and a 200 ms time lag.

micro-ECoG grids could form the basis for a neural prosthesis that provides rapid and intuitive communication, e.g. speech recognition and thought typing, through decoding the neural signals that intrinsically control the articulate movements of speaking and typing. Here we show that neural signals recorded from micro-ECoG grids placed on the primary motor cortex could provide control signals for articulate movements, i.e., classification of spoken words, classification of individual finger movements, and continuous decoding of hand position during reaching. Each of these decodes performed well above chance, and decode performance was influenced by the selection and combination of time and frequency domain features.

People comfortably hear and vocalize words in the range of 150–160 words per minute (Williams 1998). Our results demonstrated that classification of words from LFPs recorded on micro-ECoG grids can be performed rapidly using only 750 ms of data

yielding a maximum of 80 words per minute. The classification performed with an accuracy of 82.4% correct for 11 classes, nine times the level of chance. The relatively flat shape of the speech decode performance curve suggests that decoding a longer list of words is feasible without a large decrease in performance. However, it is likely that increasing the number of electrodes in the micro-ECoG grids, implanting grids over both hemispheres, and improvements in decoding algorithms may be needed to provide rapid and accurate decoding of larger sets of words. The decode was able to classify the silent states with the highest accuracy, most likely due to an absence of increased voltage or power during these periods. Differentiating between speech and silence states, i.e., detecting the intention to speak, would be an important component for any practical communication device for patients.

For finger flexion classification, the decode performed above chance for all patients. Sessions with patients were very limited in time both because of clinical needs and because of the general well-being of the patient directly after invasive brain surgery. Therefore, the finger movement task was limited to index, middle, and ring finger flexions and rest. These basic movements demonstrated that micro-ECoG grids are capable of recording LFP activity correlated with individual finger movements without over taxing the patients. Classifying the flexion of the thumb, the extension of fingers, and combined finger movements will be an important next step in demonstrating useful control of a prosthetic hand. The decode performance was lowest for Patient E. We observed that Patient E had difficulty making finger movements, which may have contributed to the relatively poor decode performance. The confusion matrix in Figure 3.4B demonstrates that index and ring finger flexion were inaccurately decoded several

times. More precise methods for monitoring finger movement and force could capture subtle stabilization movements that may have confounded the decode algorithm. For Patients C, D, and E, rest was classified with the highest accuracy probably due to an absence of increased LFP activity that was present with finger movement. Detection and classification of finger movement would be an important component for practical prosthetic arm control (Egan et al. 2012).

This study demonstrated that the continuous decode of arm movement is possible using micro-ECoG grids to record LFPs. Significant work remains to improve the accuracy and performance of the Kalman filter decode. Due to significant nonstationarities in neural signals, it is necessary to retrain decode algorithms over time. Specifically, adaptive methods could be applied to the LFP features to update the parameters A, H, W, and Q to reflect changing relationships in the LFP data over time. The recalibrated feedback intention-trained Kalman filter (ReFIT-KF) algorithm has demonstrated high performance for 2-Dimension tasks without retraining (Gilja et al. 2012). Furthermore, although the linear models used for this work were sufficient for an initial demonstration, the true nature of the relationship between motor output and LFP activity is likely nonlinear, and therefore the extended Kalman filter or other nonlinear variant may be more appropriate for future studies.

In addition to the offline analysis, an online Kalman filter was performed to demonstrate that neural signals recorded with micro-ECoG grids are capable of controlling the position of a computer cursor in real-time. Patient C only had minutes of exposure to the decode with a very short period of time for training the decode. If Patient C was able to use the online control for a longer period of time, the results may have

improved as he adapted to the real-time Kalman filter (Carmena et al. 2003). In addition, the selection of the beta band power for the LFP features was likely not ideal. Use of voltage and time domain features, as well as using power spectra of higher-frequency bands, would have likely improved online decoding performance (Zhuang et al. 2010). Power in high frequencies such as the gamma band has been shown to correlate with movement, but low-frequency activity (< 5 Hz) is thought to reflect neural processes preceding spiking activity and may provide relevant features for control over a prosthetic arm as well (Bansal et al. 2011; Logothetis 2002; Mitzdorf 1985).

The use of both time and frequency domain features increased decoding performance because the data from these two domains had nonoverlapping time periods and was binned in different manners. For the speech classification, using both the time and frequency domain provided the decode with LFP features in the time domain that were lower frequency (below 100 Hz) for 250 ms before the onset of articulation to the 500 ms after, and with LFP features in the frequency domain that were a broader range of frequencies (1 to 1000 Hz) for the onset of articulation to 500 ms after. For the finger flexion classification, using both the time domain and time varying power in the frequency domain provided the decode with LFP features in the time domain that were lower frequency (below 100 Hz) and with LFP features in the frequency domain between 65 to 115 Hz. For the continuous arm movement decode, there was only a small increase in the decode performance with LFP features from both the time and time varying frequency domain. Because continuous decodes integrate the features over small time windows, it is difficult to compare the results of continuous versus discrete decodes.

Neural activity and behavioral tasks were recorded from each patient over a short

one- to two-week period. The patients' ability to participate in the experiments were restricted to what they could do while lying in a bed, and were additionally impacted by their changing medical status and the preeminent need to provide care and treatment. Therefore, the time to run the experiments was limited and experimental sessions had to be conducted with great efficiency. Ideally, more trials would be obtained and tasks would include more complex movements; and all decodes could be implemented online to allow for real-time sensory feedback. The patients involved in this study suffered from medically refractory epilepsy for many years and areas of the motor cortex may have been abnormally mapped (Lado et al. 2002; Teskey et al. 2002), which is an important consideration when transitioning to a different patient population.

Generally, the decode performance for patients implanted with micro-ECoG grids manufactured by PMT was higher than the decode performance for patients implanted with micro-ECoG grids manufactured by Ad-Tech. The wires forming the electrodes in PMT grids terminated in small protuberances of silicone, which may have pushed against the arachnoid layer resulting in better contact with the cerebral cortex and stabilizing the position of the grid relative to the cortex. The wires forming the electrodes in Ad-Tech grids terminated flush with or slightly protruding from the silicone base, which may have allowed cerebrospinal fluid to accumulate between the electrode and the cerebral cortex. The accumulation of cerebrospinal fluid increases electrical shunting between electrodes and a higher correlation of neural signals between electrodes (Kellis et al. 2011). Due to the silicone protuberances and the microwires extending above the silicone base of the grids, great care was taken to not slide the grids along the surface of the cortex.

This study demonstrates while the size of micro-ECoG electrodes is well suited to

record relevant information, improvements can be made with these devices. Manufacturing micro-ECoG grids that either protrude slightly in a safe way or are made of a material that conforms to the cortex surface may prevent grid movement and cerebrospinal fluid from accumulating between the cortex and the micro-ECoG grid. Thinner micro-ECoG grids are currently being designed to have increased flexibility using materials such as polyimide (Thongpang et al. 2011; Viventi et al. 2011) or PDMS (Ochoa et al. 2013). Increased spatial coverage of the grid by adding more electrodes would increase the number of relevant neural signals and allow better decoding accuracy. Larger coverage area would increase the probability of placing the grid in the optimum location given patient-to-patient variability and possible abnormal mapping due to neurological disorders. However, the increased grid size would increase the number of electrodes and require a recording system with increased bandwidth and storage for the larger volume of data. Ideally, thinner and larger wireless micro-ECoG grids would be implanted chronically in patients with severe paralysis or locked-in syndrome to provide control signals for highly articulate prosthetic devices.

This study provides further evidence that there is significant motor information represented at the scale of single cortical columns and a micro-ECoG grid is capable of acquiring LFP signals at this scale from the surface of the cortex (Chestek et al. 2013; Kellis et al. 2011; Kellis et al. 2012; Kellis et al. 2010a). By providing high spatial and temporal resolution recordings of neocortical activity, micro-ECoG grids are a promising neural interface for providing articulate and intuitive control for communication or prosthetic devices.

3.6 References

Bansal AK, Vargas-Irwin CE, Truccolo W, and Donoghue JP. Relationships among Low-Frequency Local Field Potentials, Spiking Activity, and Three-Dimensional Reach and Grasp Kinematics in Primary Motor and Ventral Premotor Cortices. *J Neurophysiol* 105: 1603-1619, 2011.

Barrese JC, Rao N, Paroo K, Triebwasser C, Vargas-Irwin C, Franquemont L, and Donoghue JP. Failure Mode Analysis of Silicon-Based Intracortical Microelectrode Arrays in Non-Human Primates. *J Neural Eng* 10: 066014, 2013.

Birbaumer N. Breaking the Silence: Brain-Computer Interfaces (Bci) for Communication and Motor Control. *Psychophysiology* 43: 517-532, 2006.

Birbaumer N, Ghanayim N, Hinterberger T, Iversen I, Kotchoubey B, Kubler A, Perelmouter J, Taub E, and Flor H. A Spelling Device for the Paralysed. *Nature* 398: 297-298, 1999.

Blakely T, Miller KJ, Rao RP, Holmes MD, and Ojemann JG. Localization and Classification of Phonemes Using High Spatial Resolution Electrocorticography (Ecog) Grids. *Conf Proc IEEE Eng Med Biol Soc* 2008: 4964-4967, 2008.

Buzsaki G, Anastassiou CA, and Koch C. The Origin of Extracellular Fields and Currents--Eeg, Ecog, Lfp and Spikes. *Nat Rev Neurosci* 13: 407-420, 2012.

Carmena JM, Lebedev MA, Crist RE, O'Doherty JE, Santucci DM, Dimitrov DF, Patil PG, Henriquez CS, and Nicolelis MA. Learning to Control a Brain-Machine Interface for Reaching and Grasping by Primates. *PLoS Biol* 1: E42, 2003.

Chang EF, Rieger JW, Johnson K, Berger MS, Barbaro NM, and Knight RT. Categorical Speech Representation in Human Superior Temporal Gyrus. *Nat Neurosci* 13: 1428-1432, 2010.

Chao ZC, Nagasaka Y, and Fujii N. Long-Term Asynchronous Decoding of Arm Motion Using Electrocorticographic Signals in Monkeys. *Front Neuroeng* 3: 3, 2010.

Chestek CA, Gilja V, Blabe CH, Foster BL, Shenoy KV, Parvizi J, and Henderson JM. Hand Posture Classification Using Electrocorticography Signals in the Gamma Band over Human Sensorimotor Brain Areas. *J Neural Eng* 10: 026002, 2013.

Chestek CA, Gilja V, Nuyujukian P, Foster JD, Fan JM, Kaufman MT, Churchland MM, Rivera-Alvidrez Z, Cunningham JP, Ryu SI, and Shenoy KV. Long-Term Stability of Neural Prosthetic Control Signals from Silicon Cortical Arrays in Rhesus Macaque Motor Cortex. *J Neural Eng* 8: 045005, 2011.

Collinger JL, Wodlinger B, Downey JE, Wang W, Tyler-Kabara EC, Weber DJ, McMorland AJ, Velliste M, Boninger ML, and Schwartz AB. High-Performance Neuroprosthetic Control by an Individual with Tetraplegia. *Lancet* 381: 557-564, 2013.

Cooper R, et al. Comparison of Subcortical, Cortical and Scalp Activity Using Chronically Indwelling Electrodes in Man. *Electroencephalogr Clin Neurophysiol* 18: 217-228, 1965.

Crone N, Sinai, A., Korzeniewska, A. *Event-Related Dynamics of Brain Oscillations*. Elsevier, 2006.

Egan J, Baker J, House PA, and Greger B. Decoding Dexterous Finger Movements in a Neural Prosthesis Model Approaching Real-World Conditions. *IEEE Trans Neural Syst Rehabil Eng* 20: 836-844, 2012.

Felton EA, Radwin RG, Wilson JA, and Williams JC. Evaluation of a Modified Fitts Law Brain-Computer Interface Target Acquisition Task in Able and Motor Disabled Individuals. *J Neural Eng* 6: 056002, 2009.

Fraser GW, Chase SM, Whitford A, and Schwartz AB. Control of a Brain-Computer Interface without Spike Sorting. *J Neural Eng* 6: 055004, 2009.

Ganguly K, Secundo L, Ranade G, Orsborn A, Chang EF, Dimitrov DF, Wallis JD, Barbaro NM, Knight RT, and Carmena JM. Cortical Representation of Ipsilateral Arm Movements in Monkey and Man. *J Neurosci* 29: 12948-12956, 2009.

Gilja V, Nuyujukian P, Chestek CA, Cunningham JP, Yu BM, Fan JM, Churchland MM, Kaufman MT, Kao JC, Ryu SI, and Shenoy KV. A High-Performance Neural Prosthesis Enabled by Control Algorithm Design. *Nat Neurosci* 15: 1752-1757, 2012.

Guenther FH, Brumberg JS, Wright EJ, Nieto-Castanon A, Tourville JA, Panko M, Law R, Siebert SA, Bartels JL, Andreasen DS, Ehirim P, Mao H, and Kennedy PR. A Wireless Brain-Machine Interface for Real-Time Speech Synthesis. *PLoS One* 4: e8218, 2009.

Hazrati M, and Erfanian A. An Online Eeg-Based Brain-Computer Interface for Controlling Hand Grasp Using an Adaptive Probabilistic Neural Network. *Med Eng Phys* 32: 730-739, 2010.

Hochberg LR, Bacher D, Jarosiewicz B, Masse NY, Simeral JD, Vogel J, Haddadin S, Liu J, Cash SS, van der Smagt P, and Donoghue JP. Reach and Grasp by People with Tetraplegia Using a Neurally Controlled Robotic Arm. *Nature* 485: 372-375, 2012.

Huang D, Lin P, Fei DY, Chen X, and Bai O. Decoding Human Motor Activity from Eeg Single Trials for a Discrete Two-Dimensional Cursor Control. *J Neural Eng* 6: 046005, 2009.

Katzner S, Nauhaus I, Benucci A, Bonin V, Ringach DL, and Carandini M. Local Origin of Field Potentials in Visual Cortex. *Neuron* 61: 35-41, 2009.

Kellis S, Greger B, Hanrahan S, House P, and Brown R. Sensing Millimeter-Scale Dynamics in Cortical Surface Potentials for Neural Prosthetics. In: *Sensors, 2011 IEEE*2011, p. 1823-1826.

Kellis S, Hanrahan S, Davis T, House PA, Brown R, and Greger B. Decoding Hand Trajectories from Micro-Electrocorticography in Human Patients. *Conf Proc IEEE Eng Med Biol Soc* 2012: 4091-4094, 2012.

Kellis S, Miller K, Thomson K, Brown R, House P, and Greger B. Classification of Spoken Words Using Surface Local Field Potentials. *Conf Proc IEEE Eng Med Biol Soc* 2010: 3827-3830, 2010a.

Kellis S, Miller K, Thomson K, Brown R, House P, and Greger B. Decoding Spoken Words Using Local Field Potentials Recorded from the Cortical Surface. *J Neural Eng* 7: 056007, 2010b.

Kellis SS, House PA, Thomson KE, Brown R, and Greger B. Human Neocortical Electrical Activity Recorded on Nonpenetrating Microwire Arrays: Applicability for Neuroprostheses. *Neurosurg Focus* 27: E9, 2009.

Khawaja FA, Tsui JM, and Pack CC. Pattern Motion Selectivity of Spiking Outputs and Local Field Potentials in Macaque Visual Cortex. *J Neurosci* 29: 13702-13709, 2009.

Kim J, Wilson JA, and Williams JC. A Cortical Recording Platform Utilizing Microecog Electrode Arrays. *Conf Proc IEEE Eng Med Biol Soc* 2007: 5353-5357, 2007.

Kim SP, Simeral JD, Hochberg LR, Donoghue JP, Friehs GM, and Black MJ. Point-and-Click Cursor Control with an Intracortical Neural Interface System by Humans with Tetraplegia. *IEEE Trans Neural Syst Rehabil Eng* 19: 193-203, 2011.

Kubanek J, Miller KJ, Ojemann JG, Wolpaw JR, and Schalk G. Decoding Flexion of Individual Fingers Using Electrocorticographic Signals in Humans. *J Neural Eng* 6: 066001, 2009.

Lado FA, Legatt AD, LaSala PA, and Shinnar S. Alteration of the Cortical Motor Map in a Patient with Intractable Focal Seizures. *J Neurol Neurosurg Psychiatry* 72: 812-815, 2002.

Lauer RT, Peckham PH, and Kilgore KL. Eeg-Based Control of a Hand Grasp Neuroprosthesis. *Neuroreport* 10: 1767-1771, 1999.

Leuthardt EC, Freudenberg Z, Bundy D, and Roland J. Microscale Recording from Human Motor Cortex: Implications for Minimally Invasive Electrocorticographic Brain-Computer Interfaces. *Neurosurg Focus* 27: E10, 2009.

Leuthardt EC, Gaona C, Sharma M, Szrama N, Roland J, Freudenberg Z, Solis J, Breshears J, and Schalk G. Using the Electrocorticographic Speech Network to Control a Brain-Computer Interface in Humans. *J Neural Eng* 8: 036004, 2011.

Leuthardt EC, Schalk G, Wolpaw JR, Ojemann JG, and Moran DW. A Brain-Computer Interface Using Electrocorticographic Signals in Humans. *J Neural Eng* 1: 63-71, 2004.

Logothetis NK. The Neural Basis of the Blood-Oxygen-Level-Dependent Functional Magnetic Resonance Imaging Signal. *Philos Trans R Soc Lond B Biol Sci* 357: 1003-1037, 2002.

Menon V, Freeman WJ, Cutillo BA, Desmond JE, Ward MF, Bressler SL, Laxer KD, Barbaro N, and Gevins AS. Spatio-Temporal Correlations in Human Gamma Band Electrocorticograms. *Electroencephalogr Clin Neurophysiol* 98: 89-102, 1996.

Milekovic T, Fischer J, Pistohl T, Ruescher J, Schulze-Bonhage A, Aertsen A, Rickert J, Ball T, and Mehring C. An Online Brain-Machine Interface Using Decoding of Movement Direction from the Human Electrocorticogram. *J Neural Eng* 9: 046003, 2012.

Miller KJ, Hermes D, Honey CJ, Hebb AO, Ramsey NF, Knight RT, Ojemann JG, and Fetz EE. Human Motor Cortical Activity Is Selectively Phase-Entrained on Underlying Rhythms. *PLoS Comput Biol* 8: e1002655, 2012.

Miller KJ, Leuthardt EC, Schalk G, Rao RP, Anderson NR, Moran DW, Miller JW, and Ojemann JG. Spectral Changes in Cortical Surface Potentials During Motor Movement. *J Neurosci* 27: 2424-2432, 2007.

Miller KJ, Zanos S, Fetz EE, den Nijs M, and Ojemann JG. Decoupling the Cortical Power Spectrum Reveals Real-Time Representation of Individual Finger Movements in Humans. *J Neurosci* 29: 3132-3137, 2009.

Mitra P, and Bokil H. *Observed Brain Dynamics*. Oxford ; New York: Oxford University Press, 2008, p. xxii, 381 p.

Mitzdorf U. Current Source-Density Method and Application in Cat Cerebral Cortex: Investigation of Evoked Potentials and Eeg Phenomena. *Physiol Rev* 65: 37-100, 1985.

Mountcastle VB. An Organizing Principle for Cerebral Function: The Unit Module and the Distributed System. In: *The Mindful Brain*, edited by G. M. Edelman VBM. Massachusetts: MIT Press, 1978, p. pp. 7–50.

Nunez PL, and Srinivasan R. A Theoretical Basis for Standing and Traveling Brain Waves Measured with Human Eeg with Implications for an Integrated Consciousness. *Clin Neurophysiol* 117: 2424-2435, 2006.

Ochoa M, Wei P, Wolley AJ, Otto KJ, and Ziaie B. A Hybrid Pdms-Parylene Subdural Multi-Electrode Array. *Biomed Microdevices* 15: 437-443, 2013.

Pfurtscheller G, Guger C, Muller G, Krausz G, and Neuper C. Brain Oscillations Control Hand Orthosis in a Tetraplegic. *Neurosci Lett* 292: 211-214, 2000.

Pistohl T, Ball T, Schulze-Bonhage A, Aertsen A, and Mehring C. Prediction of Arm Movement Trajectories from Ecog-Recordings in Humans. *J Neurosci Methods* 167: 105-114, 2008.

Pistohl T, Schmidt TS, Ball T, Schulze-Bonhage A, Aertsen A, and Mehring C. Grasp Detection from Human Ecog During Natural Reach-to-Grasp Movements. *PLoS One* 8: e54658, 2013.

Pistohl T, Schulze-Bonhage A, Aertsen A, Mehring C, and Ball T. Decoding Natural Grasp Types from Human Ecog. *Neuroimage* 59: 248-260, 2012.

Sanchez JC, Gunduz A, Carney PR, and Principe JC. Extraction and Localization of Mesoscopic Motor Control Signals for Human Ecog Neuroprosthetics. *J Neurosci Methods* 167: 63-81, 2008.

Schalk G, McFarland DJ, Hinterberger T, Birbaumer N, and Wolpaw JR. Bci2000: A General-Purpose Brain-Computer Interface (Bci) System. *IEEE Trans Biomed Eng* 51: 1034-1043, 2004.

Schalk G, Miller KJ, Anderson NR, Wilson JA, Smyth MD, Ojemann JG, Moran DW, Wolpaw JR, and Leuthardt EC. Two-Dimensional Movement Control Using Electrocorticographic Signals in Humans. *J Neural Eng* 5: 75-84, 2008.

Schendel AA, Thongpang S, Brodnick SK, Richner TJ, Lindevig BD, Krugner-Higby L, and Williams JC. A Cranial Window Imaging Method for Monitoring Vascular Growth around Chronically Implanted Micro-Ecog Devices. *J Neurosci Methods* 218: 121-130, 2013.

Simeral JD, Kim SP, Black MJ, Donoghue JP, and Hochberg LR. Neural Control of Cursor Trajectory and Click by a Human with Tetraplegia 1000 Days after Implant of an Intracortical Microelectrode Array. *J Neural Eng* 8: 025027, 2011.

Slutzky MW, Jordan LR, Krieg T, Chen M, Mogul DJ, and Miller LE. Optimal Spacing of Surface Electrode Arrays for Brain-Machine Interface Applications. *J Neural Eng* 7: 26004, 2010.

Smith E, and Delargy M. Locked-in Syndrome. *BMJ* 330: 406-409, 2005.

Stacey WC, Kellis S, Patel PR, Greger B, and Butson CR. Signal Distortion from Microelectrodes in Clinical Eeg Acquisition Systems. *J Neural Eng* 9: 056007, 2012.

Teskey GC, Monfils MH, VandenBerg PM, and Kleim JA. Motor Map Expansion Following Repeated Cortical and Limbic Seizures Is Related to Synaptic Potentiation. *Cereb Cortex* 12: 98-105, 2002.

Thongpang S, Richner TJ, Brodnick SK, Schendel A, Kim J, Wilson JA, Hippensteel J, Krugner-Higby L, Moran D, Ahmed AS, Neimann D, Sillay K, and

Williams JC. A Micro-Electrocorticography Platform and Deployment Strategies for Chronic Bci Applications. *Clin EEG Neurosci* 42: 259-265, 2011.

Tsanov M, Chah E, Wright N, Vann SD, Reilly R, Erichsen JT, Aggleton JP, and O'Mara SM. Oscillatory Entrainment of Thalamic Neurons by Theta Rhythm in Freely Moving Rats. *J Neurophysiol* 105: 4-17, 2011.

Van Gompel JJ, Stead SM, Giannini C, Meyer FB, Marsh WR, Fountain T, So E, Cohen-Gadol A, Lee KH, and Worrell GA. Phase I Trial: Safety and Feasibility of Intracranial Electroencephalography Using Hybrid Subdural Electrodes Containing Macro- and Microelectrode Arrays. *Neurosurg Focus* 25: E23, 2008.

Viventi J, Kim DH, Vigeland L, Frechette ES, Blanco JA, Kim YS, Avrin AE, Tiruvadi VR, Hwang SW, Vanleer AC, Wulsin DF, Davis K, Gelber CE, Palmer L, Van der Spiegel J, Wu J, Xiao J, Huang Y, Contreras D, Rogers JA, and Litt B. Flexible, Foldable, Actively Multiplexed, High-Density Electrode Array for Mapping Brain Activity in Vivo. *Nat Neurosci* 14: 1599-1605, 2011.

Wang W, Collinger JL, Degenhart AD, Tyler-Kabara EC, Schwartz AB, Moran DW, Weber DJ, Wodlinger B, Vinjamuri RK, Ashmore RC, Kelly JW, and Boninger ML. An Electrocorticographic Brain Interface in an Individual with Tetraplegia. *PLoS One* 8: e55344, 2013.

Williams JR. Guidelines for the Use of Multimedia in Instruction. *Proceedings of the Human Factors and Ergonomics Society 42nd Annual Meeting* 1447–1451, 1998.

Wolpaw JR, and McFarland DJ. Control of a Two-Dimensional Movement Signal by a Noninvasive Brain-Computer Interface in Humans. *Proc Natl Acad Sci U S A* 101: 17849-17854, 2004.

Worrell GA, Gardner AB, Stead SM, Hu S, Goerss S, Cascino GJ, Meyer FB, Marsh R, and Litt B. High-Frequency Oscillations in Human Temporal Lobe: Simultaneous Microwire and Clinical Macroelectrode Recordings. *Brain* 131: 928-937, 2008.

Wu W, Gao Y, Bienenstock E, Donoghue JP, and Black MJ. Bayesian Population Decoding of Motor Cortical Activity Using a Kalman Filter. *Neural Comput* 18: 80-118, 2006.

Zhuang J, Truccolo W, Vargas-Irwin C, and Donoghue JP. Decoding 3-D Reach and Grasp Kinematics from High-Frequency Local Field Potentials in Primate Primary Motor Cortex. *IEEE Trans Biomed Eng* 57: 1774-1784, 2010.

CHAPTER 4

CONCLUSION

In this dissertation, microscale recordings in the human cortex were examined during the administration of propofol anesthesia and articulate movements such as speech, finger flexion, and arm reach. Through these studies, we increased our understanding of LFPs in neurophysiological recordings. In Chapter 2, we used propofol anesthesia to probe the relationship between APs and LFPs recoded with microelectrodes arrays. To examine this, we performed AP-aligned LFP analysis, which demonstrated the generation of large amplitude spike-like LFP activity in lightly and deeply anesthetized states. In addition, the temporal relationship between APs and LFPs remained relatively consistent at all levels of propofol. This study demonstrated that neurons can represent information in terms of the timing of APs relative to neuronal oscillations (the LFP). In Chapter 3, we demonstrated that significant motor information is represented at the scale of single cortical columns and a micro-ECoG grid is capable of acquiring LFP signals at this scale from the surface of the cortex. LFPs are very informative signals, but the term LFP is widely used for microelectrode, ECoG, and EEG recordings. Although ECoG and EEG record field potentials from neural tissue, EEG and ECoG electrodes have a higher surface area, lower impedance, and therefore record electrical activity from a much larger area of neural tissue. It is difficult to compare the signals recorded by different

modalities, because studies vary in the behavioral task used, the location of the electrode grid, and subject variability. A study in which one subject has simultaneous recordings from EEG, ECoG, surface microelectrodes, and penetrating microelectrodes would be able to thoroughly quantify specific abilities and limitations of each recording modality.

Recording the neural activity of human subjects is indispensable for fundamental neuroscience research and clinical applications. Human neurophysiological studies have limitations that must be considered. Addressing these challenges such as the type of subjects and neural interfaces used can further our knowledge of neural mechanisms and improve medical technology.

4.1 Challenges: Subjects

In the field of invasive recordings of neocortical activity in humans, subjects are primarily patients suffering from medically refractory epilepsy. Experimental sessions with patients are very limited in time both because of clinical needs and because of the need to preserve general well-being of the patient directly after invasive brain surgery. Clinical needs and constraints drive the placement of electrodes used for research, limiting the types of experiments that can be performed. Furthermore, behavioral paradigms are restricted to movements the patient can perform while lying in a hospital bed and tethered to recording equipment. Wireless recording setups could provide greater movement and comfort for these patients leading to better experimental sessions (Miranda et al. 2010). The impact of epilepsy in these subjects is also important to consider when recording neocortical activity. Neural recordings during experimental sessions must be reviewed for seizure activity and interictal discharges. In addition,

relevant cortices such as motor areas and speech areas may be abnormally mapped.

Subject recruitment is limited to the small number of patients who are undergoing long-term monitoring for their epilepsy and who have volunteered for the research study. For each patient, the location of possible areas for neural recordings is different. Therefore, collaborating with other research labs will be valuable for the future of invasive neurophysiological studies in human subjects. One such initiative is the International Epilepsy Electrophysiology Portal (IEEG-Portal), which is a platform for sharing data and tools for studies relevant to epilepsy (Litt et al. 2012). There are many preventative measures that must be put into place such as de-identifying data for patient's privacy, approval of the research study by the IRB of the institution, and formatting the data in a standard way for universal use.

Recording microscale neocortical activity in patients without epilepsy is also important. To assess BCI systems for the end user, we must implant microelectrode arrays in people who are paralyzed and have them drive communication or control systems for clinical trials. Recent studies have safely implanted ECoG grids (Wang et al. 2013) and penetrating microelectrode arrays (Collinger et al. 2013; Hochberg et al. 2012) in patients with tetraplegia.

4.2 Challenges: Neural Interfaces

To record neocortical activity in patients, researchers want effective, reliable, and safe electrodes. Improvements can be made with the penetrating microelectrode arrays and micro-ECoG grids used in this dissertation. Penetrating microelectrode arrays are limited in their use in epilepsy patients due to their increased invasiveness. These electrodes are

also limited in their spatial coverage (4mm x 4 mm). The grid design could have increased spatial coverage by adding more electrodes or increasing interelectrode spacing. Increasing the number of electrodes would require a recording system with increased bandwidth and storage for the larger volume of data and increasing interelectrode spacing may lead to missed relevant neural signals. Furthermore, neural signals recorded from penetrating microelectrode arrays have been shown to degrade over time.

Electrode grids placed on the surface of the cortex may record signals that are more reliable over time. This dissertation demonstrates that while the size of micro-ECoG electrodes is well suited to record relevant information, improvements can be made with these devices. Manufacturing micro-ECoG grids that either protrude slightly in a safe way or are made of a material that conforms to the cortical surface may prevent grid movement and cerebrospinal fluid from accumulating between the cortex and the micro-ECoG grid. These designs would limit implantation techniques and grids could not be slid along the surface of the cortex like traditional ECoG grids. Thinner micro-ECoG grids are currently being designed to have increased flexibility using materials such as polyimide (Thongpang et al. 2011; Viventi et al. 2011) or PDMS (Ochoa et al. 2013). A thinner design would avoid placing extra pressure on the cortex or blood vessels and a flexible design may be able to reach relevant neural signals located in both gyri and sulci. However, FDA approval of this new technology and implantation in humans for clinical trials is years away. In addition, increased spatial coverage of the grid by adding more electrodes would increase the number of relevant neural signals and allow better decoding accuracy. Larger coverage area would increase the probability of placing the

grid in the optimum location given patient-to-patient variability and possible abnormal mapping due to neurological disorders. Ideally, thinner and larger wireless micro-ECoG grids would be used for human neurophysiological research.

4.3 Conclusion

In this dissertation, microscale neural activity was recorded from human subjects during the administration of propofol anesthesia and articulate movements such as speech, finger flexion, and arm reach.

In Chapter 2, with the administration of propofol, we consistently observed a decrease in high-frequency power and AP firing rate, and an increase in regular and predictable patterns of LFP and AP activity. This reduced information processing capacity in the neocortex was correlated with a loss of responsiveness and consciousness. These results have important implications for the processing of information in the neocortex, and therefore on the interpretation of experimental results in anesthetized preparations and clinical results in intraoperative cortical mapping.

The findings in Chapter 3 provide further evidence that there is significant motor information represented at the scale of single cortical columns and a micro-ECoG grid is capable of acquiring LFP signals at this scale from the surface of the cortex. By providing high spatial and temporal resolution recordings of neocortical activity, micro-ECoG grids are a promising tool to provide articulate and intuitive control for communication or control systems.

4.4 References

Collinger JL, Wodlinger B, Downey JE, Wang W, Tyler-Kabara EC, Weber DJ, McMorland AJ, Velliste M, Boninger ML, and Schwartz AB. High-Performance Neuroprosthetic Control by an Individual with Tetraplegia. *Lancet* 381: 557-564, 2013.

Hochberg LR, Bacher D, Jarosiewicz B, Masse NY, Simeral JD, Vogel J, Haddadin S, Liu J, Cash SS, van der Smagt P, and Donoghue JP. Reach and Grasp by People with Tetraplegia Using a Neurally Controlled Robotic Arm. *Nature* 485: 372-375, 2012.

Litt B, Worrell G, and Ives Z. International Epilepsy Electrophysiological Portal http://ieeg.org.

Miranda H, Gilja V, Chestek CA, Shenoy KV, and Meng TH. Hermesd: A High-Rate Long-Range Wireless Transmission System for Simultaneous Multichannel Neural Recording Applications. *IEEE Trans Biomed Circuits Syst* 4: 181-191, 2010.

Ochoa M, Wei P, Wolley AJ, Otto KJ, and Ziaie B. A Hybrid Pdms-Parylene Subdural Multi-Electrode Array. *Biomed Microdevices* 15: 437-443, 2013.

Thongpang S, Richner TJ, Brodnick SK, Schendel A, Kim J, Wilson JA, Hippensteel J, Krugner-Higby L, Moran D, Ahmed AS, Neimann D, Sillay K, and Williams JC. A Micro-Electrocorticography Platform and Deployment Strategies for Chronic Bci Applications. *Clin EEG Neurosci* 42: 259-265, 2011.

Viventi J, Kim DH, Vigeland L, Frechette ES, Blanco JA, Kim YS, Avrin AE, Tiruvadi VR, Hwang SW, Vanleer AC, Wulsin DF, Davis K, Gelber CE, Palmer L, Van der Spiegel J, Wu J, Xiao J, Huang Y, Contreras D, Rogers JA, and Litt B. Flexible, Foldable, Actively Multiplexed, High-Density Electrode Array for Mapping Brain Activity in Vivo. *Nat Neurosci* 14: 1599-1605, 2011.

Wang W, Collinger JL, Degenhart AD, Tyler-Kabara EC, Schwartz AB, Moran DW, Weber DJ, Wodlinger B, Vinjamuri RK, Ashmore RC, Kelly JW, and Boninger ML. An Electrocorticographic Brain Interface in an Individual with Tetraplegia. *PLoS One* 8: e55344, 2013.